Surfaces and Interfaces 14 (2019) 222–237

Contents lists available at ScienceDirect

Surfaces and Interfaces

journal homepage: www.elsevier.com/locate/surfin

Corrosion protection of carbon steel by two newly synthesized benzimidazol-2-ones substituted 8-hydroxyquinoline derivatives in 1 M HCl: Experimental and theoretical study

Mohamed El Faydy[a], Mohamed Rbaa[a], Loubna Lakhrissi[a], Brahim Lakhrissi[a], Ismail Warad[b], Abdelkader Zarrouk[c,*], Ime Bassey Obot[d]

[a] Laboratory of Agricultural Resources, Polymer and Process Engineering, Department of Chemistry, Faculty of Sciences, Ibn Tofail University, PO Box 133, 14000 Kenitra, Morocco
[b] Department of Chemistry, AN-Najah National University, P.O. Box 7, Nablus, Palestine
[c] Laboratory of Materials, Nanotechnology and Environment, Faculty of Sciences, Mohammed V University, Av. Ibn Battouta, PO Box 1014 Agdal, Rabat, Morocco
[d] Center of Research Excellence in Corrosion, Research Institute, King Fahd University of Petroleum and Minerals, Dhahran 31261, Saudi Arabia

ARTICLE INFO

Keywords:
Synthesis
NMR
Carbon steel
Corrosion Inhibition
Electrochemical techniques
Monte Carlo simulations

ABSTRACT

Two new organic compounds composed of 8-hydroxyquinoline and benzimidazol-2-one units have been successfully prepared, and identified by different spectroscopic methods (IR, NMR and Elemental analysis). The synthesized heterocyclic namely 1-((8-hydroxyquinolin-5-yl)methyl)-3-(prop-1-en-2-yl)-1H-benzimidazol-2(3H)-one (HMPB) and 1,3-bis((8-hydroxy-quinolin-5-yl)methyl)-1H-benzimidazol-2(3H)-one (BHMB) are assessed as corrosion inhibitors for carbon steel (CS) in 1 M hydrochloric acid media utilizing gravimetric measurements, electrochemical impedance spectroscopy, potentiodynamic polarization and UV − visible spectroscopy at 298 K. The inhibiting action is more pronounced by BHMB compared to HMPB and affected a maximum value of 91% at the 10^{-3} M attributed to BHMB and 89% achieved by HMPB, the shift in corrosion potentials obtained suggested that the two compounds are cathodic-type inhibitors. The adsorption of benzimidazol-2-ones substituted 8-hydroxy-quinoline derivatives on the carbon steel surface follows the Langmuir adsorption isotherm and was found to involve chemisorption. The EIS spectra expressed principally as a slightly depressed semi-circle shape corresponding to a single time constant in Bode diagrams for the two organic compounds in the both concentration and temperature effects. In addition, all thermodynamic parameters such as ΔG°_{ads} E_a, ΔS_a and ΔH_a were estimated and discussed. Finally, the combination of density functional theory (DFT) and Monte Carlo simulations were used to understand the regions in the BHMB and HMPB molecules where interaction with steel surface can occur.

1. Introduction

Many material, exposed to its environment, corrodes over time. The phenomena of corrosion depend on a large number of complex factors such as temperature, the nature and structure of the material and the medium [1]. In order to slow the rate of the corrosion, many researchers have shifted their attention to the development of novel corrosion inhibitors based on heterocyclic organic products. These organic inhibitors act by adsorption on the metal surface by substituting water molecules to form a protective film on the metal surface [2–4]. The choice of most organic inhibitors are generally based on the electronic density on the heteroatoms like *S, N, O,* etc. [5–8]. In addition, the adsorption of organic compounds on metal surfaces is due also to the presence of the electron donating substituent, ring moiety and mesomeric effect [9,10]. In this context, a number of studies were reported with a view to understand the effect of substituent on the protective effect of organic molecules on metal surface [11–13].

Hydrochloric acid is very used in a number of industrial sectors such as removing of rust, cleaning and descaling of ferrous materials. On the other hand, carbon steel is widely used in industry and in different machinery; However, its tendency to corrode is higher when it is exposed to acids.

Benzimidazol-2-one and its derivatives are heterocyclic organic compounds have many properties ranging from biological agents to analytical chemistry and separation techniques [14–17]. So, the benzimidazol-2-one derivatives have attracted considerable attention

* Corresponding author.
E-mail address: azarrouk@gmail.com (A. Zarrouk).

https://doi.org/10.1016/j.surfin.2019.01.005
Received 11 October 2018; Received in revised form 25 December 2018; Accepted 8 January 2019
Available online 08 January 2019
2468-0230/

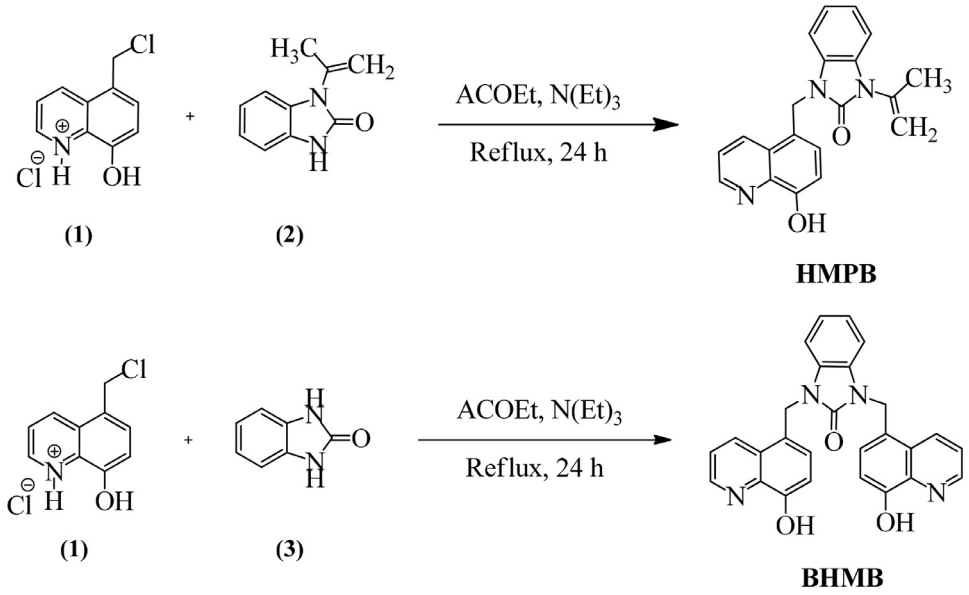

Scheme 1. the synthesis of BMHB and HMPB.

during the last few decades due to their inhibition properties for metallic corrosion [17–19].

8-hydroxyquinoline (8-HQ) is bicyclic compounds consist of two rings system: phenolic ring and pyridine ring, 8-hydroxyquinoline and its derivatives are often used as chelating agent in coordination studies and radiochemistry for metal ion extraction [20,21], the results of the literature review indicated that there is very limited researches available on corrosion inhibition of carbon steel in acid solutions by some of 8-hydroxyquinoline derivatives, with the exception of that mentioned by Achary et al. [22] and Abboud et al. [23], they have come up with that these heterocyclic molecules have moderate to good protective properties for carbon steel corrosion in Hydrochloric acid, and the protection ability reached 96% at 10^{-3} M for 5-naphthylazo-8-hydroxyquinoline and 93% at 0.7×10^{-3} M for 3-formyl-8-hydroxyquinoline. Recently, a study on the corrosion inhibition of carbon steel by 5-(chloromethyl) − 8-hydroxyquinoline hydrochloride was carried out in our laboratory. The study showed that this compound acted as a good inhibitor for XC38 steel in 1 M hydrochloric acid solution [24].

The grafting of the benzimidazolone moiety onto the 8-hydroxyquinoline molecule can make a valuable contribution to corrosion inhibition. Compounds BHMB and HMPB selected for the present investigation containing both 8-hydroxyquinoline and benzimidazolone rings in their structural moieties. They were successfully synthesized and characterized utilizing various spectroscopic methods and their anticorrosive behavior vis-a-vis carbon steel in acidic electrolyte was examined by Electrochemical methods, UV − visible spectroscopy associated with DFT methodology and Monte Carlo simulations.

2. Experimental details

2.1. Materials

Carbon steel comprises in weight %: 0.36% C; 0.10% Si; 0.01% P; 0.02% Al; 0.68% Mn; 0.005% S, 0.01% Cr and the remainder iron (Fe) was used in gravimetric and electrochemical tests. Before starting the experiments, the working electrode surface was mechanically prepared with sand paper grade from 80 to 1200. Cleaned with ethanol and dried in hot air. An electrolytic solution of 1 M HCl is produced by dilution of Hydrochloric acid 37%, AR grade with distilled water. The BHMB and HMPB selected were investigated in a wide interval of concentration ranging from 10^{-3} to 10^{-6} M, With regard to the synthesis of BMHQ and HMPB, all chemicals were obtained from Aldrich and Merck. Solvents were distilled by standard methods. The Infrared spectra of solid BHMP and HMPB were obtained by Bruker Tensor 37 FTIR Spectrometer. NMR spectra were performed on a Bruker AVANCE II 300 MHz NMR Spectrometer for solutions in Me_2SO-d_6. The Thin-layer chromatography were achieved on Silica Gel 60 RP-18 F254S (E. Merck) plates which are fluorescent at UV light of 254 nm. Melting points were obtained by Kofler hot bench of type Wagner Munz™ 50,400. Column chromatography was carried out using silica gel 60 (0.040–0.063 mm) utilizing hexane–acetone mixtures as the eluent. Elemental analyses were carried on an Elementar CHN Vario Micro Cube analyser.

Starting materials are commercially available: 8-hydroxy-5-(chloromethyl)quinolin-1-ium chloride (1) was synthesized from 8-hydroxyquinoline with formaldehyde (40%) in the presence of concentrated (37%) and gaseous hydrochloric acid as mentioned in the literature [24,25].

1-(Prop-1-en-2-yl)-benzimidazol-2-one (**2**) was synthesized from ethyl acetoacetate and *o*-phenylenediamine as described in the literature [26].

Benzimidazol-2-one (**3**) was prepared from *o*-phenylenediamine and urea as described in the literature [27].

2.2. Inhibitor preparation

The synthesized compounds **2**) and (**3**) are grafted on the 8-hydroxy-5-(chloromethyl)quinolin-1-ium chloride ((1). The outline of synthesis of HMPB and BHMB is shown in Scheme 1.

2.2.1. Synthesis section

2.2.1.1. General procedure. A mixture of benzimidazol-2-one derivatives (2 eq), 8-hydroxy-5-(chloromethyl)quinolin-1-ium chloride (1 eq) and triethylamine (2 eq) in pure ethyl acetate (40 mL) was heated under reflux. After 24 h, 3*30 mL of water was added to the mixture, extraction was carried out with 3* 10 mL of AcOEt. The organic phases were recovered, dried over anhydrous $MgSO_4$, after removal of the solvent under vacuum. The obtained residue was then purified via silica column chromatography with (n-hexane/acetone, 9:1 to 2:8, v/v), to give the desired compounds. Specific spectral information for each compound are given below.

2.2.1.2. Synthesis of 1-((8-hydroxyquinolin-5-yl)methyl) − 3-(prop-1-en-2-yl) − 1H-benzim-idazol-2(3H)-one (HMPB). 1-(prop-1-en-2-yl) − 1-

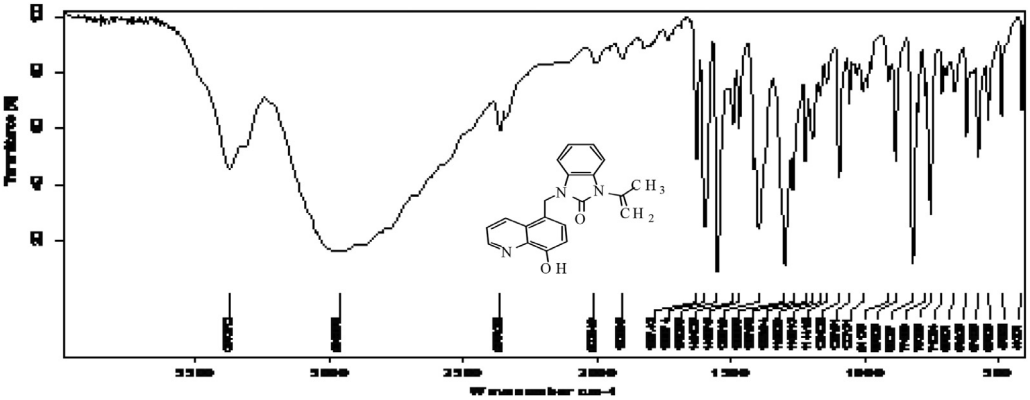

Fig. 1. IR spectrum of 1-((8-hydroxyquinolin-5-yl)methyl) – 3-(prop-1-en-2-yl) – 1H-benzim-idazol-2(3H)-one (HMPB).

benzimidazol-2-one (2) (0.76 g, 0.00436 mol) and 8-hydroxy-5-(chloromethyl)quinolin-1-ium chloride (1 g, 0.00436 mol) were used. Yield (1.05 g, 72%); white solid, mp 220 °C; IR (cm^{-1}) = 3332–2920 (-OH stretch, H bonded), 1599 and 3026 (aromatic C = C and C—H stretching), 1227 (C—N), 1623 (C = O), 1372 (C—N) (Fig. 1).

^{1}H NMR (300 MHz, DMSO-d_6), δ_{ppm} = 6.92–9.192 (m, 9 H, hydroxyquinoline and aromatic benzimidazole), 5.23 (s, 2 H,-CH_2-), 4.19 (s, 1 H, = CH_2), 4.09 (s, 1 H, = CH_2), 2.17 (s, 3 H, CH_3) (Fig. 2).

^{13}C NMR (300 MHz, DMSO-d_6), δ_{ppm} = 19.53 (CH_3), 44.15 (hydroxyquinoline -$\underline{C}H_2$-2-benzimidazolone), 82.42 (= $\underline{C}H_2$), 110.95, 122.30, 122.30, 123.51, 124.86, 127.012, 127.45, 132.80, 148.32 ($\underline{C}$H of hydroxyquinoline and benzene), 127.50, 127.80, 132.96, 139.23, 139.27, 153.30 ($\underline{C}$H of hydroxyquinoline and benzene), 162.59 ($\underline{C}$ = O amide), 148.51 (CH_3—$\underline{C}$—N) (Fig. 3).

Elemental analysis for $C_{20}H_{19}N_3O_2$: Calcd: C, 72.05; H, 5.74; N, 12.60%; Found: C, 71.92; H, 5.70; N, 12.65%.

2.2.1.3. Synthesis of 1,3-bis((8-hydroxyquinolin-5-yl)methyl) – 1H-benzimidazol-2(3H)-one (BHMB). Benzimidazol-2-one (3) (0.2927 g, 0.00218 mol) and 8-hydroxy-5-(chloromethyl)quinolin-1-ium chloride (1 g, 0.00436 mol) were used. Yield (0.64 g, 60%); white solid, mp 198 °C;

IR (cm^{-1}) = 3373–2962 (-OH stretch, H bonded), 2361, 2009 (aromatic C = C and C—H stretching), 1396 (C—N) (Fig. 4).

^{1}H NMR (300 MHz, DMSO-d_6), δ_{ppm} = 6.91–8.69 (m, 7 H of hydroxyquinoline and aromatic benzimidazolone), 5.44(s, 2H, -CH_2-) (Fig. 5).

^{13}C NMR (300 MHz, DMSO-d_6), δ_{ppm} = 48.96 (hydroxyquinoline-$\underline{C}H_2$-2-benzimidazolone), 110.17, 11.54, 118.09, 121.70, 127.85, 129.08, 148.54 ($\underline{C}$H of hydroxyquinoline and benzimidazolone), 122.20, 134.21, 136.41, 148.17, 153.71 ($\underline{C}$ of hydroxyquinoline and benzimidazolone), 162.72 ($\underline{C}$ = O) (Fig. 6).

Elemental analysis for $C_{22}H_{22}N_4O_3$: Calcd: C, 71.99; H, 4.92; N, 12.44%; Found: C, 71.82; H, 4.99; N, 12.43%.

2.3. Gravimetric study

The gravimetric tests were carried out according to ASTM G1-03 standard [28]. Weight loss testing was performed on specimens with a size of 4 cm × 1 cm × 0.2 cm. Gravimetric experiment was conducted by placing the coupons into the test solutions for 6 h and replicated three times in each concentration for reproducibility. Average weight loss was reported.

2.4. Electrochemical corrosion studies

The electrochemical experiments were conducted in a complete electrochemical cell - BEC / EDI Radiometer. The working electrode

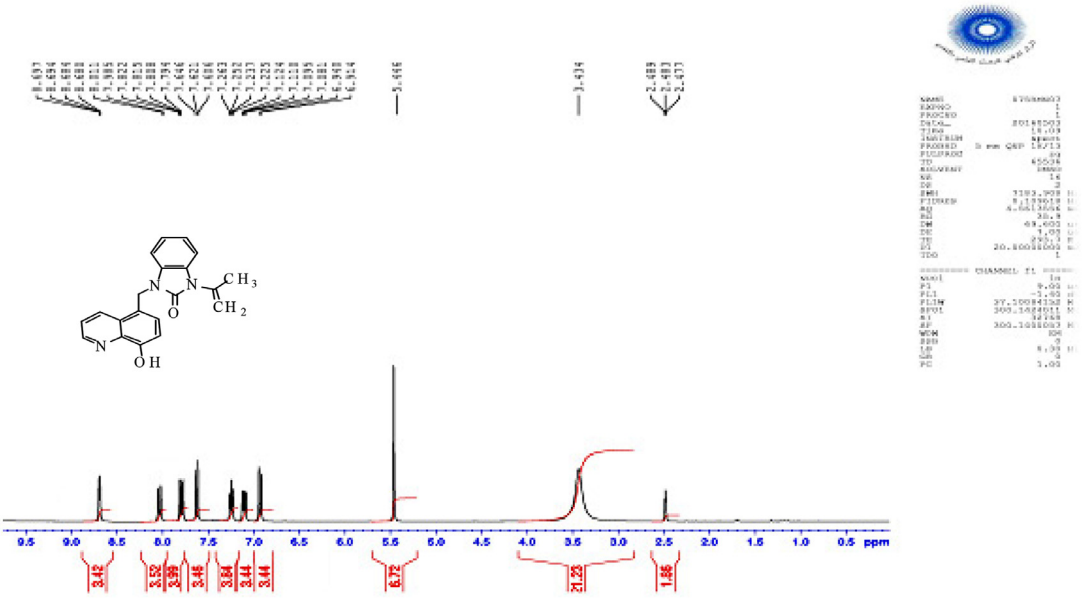

Fig. 2. ^{1}H NMR spectrum of 1-((8-hydroxyquinolin-5-yl)methyl) – 3-(prop-1-en-2-yl) – 1H-benzim-idazol-2(3H)-one (HMPB) (in DMSO-d6).

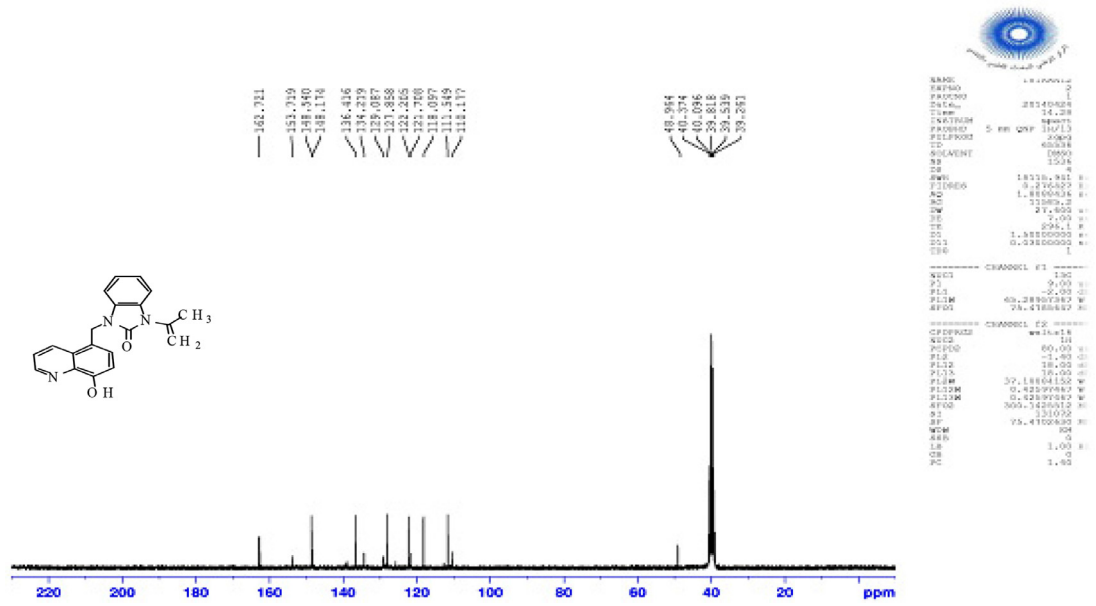

Fig. 3. ^{13}C NMR spectrum of 1-((8-hydroxyquinolin-5-yl)methyl) − 3-(prop-1-en-2-yl) − 1H-benzim-idazol-2(3H)-one (HMPB) (in DMSO-d6).

was steel with the surface area of 1 cm^2. Platinum and silver/silver chloride was used as a counter and a reference electrode (Ag/AgCl), respectively. Before recording each curve, the carbon steel sample was immersed into the prepared electrolyte for 30 min until a steady state open circuit potential (E_{ocp}) was achieved. The potentiodynamic polarization curves were obtained using VoltaLab PGZ 100 from −900 to −100(Vs. AgCl) under deaerated solution conditions with a scan rate of 0.5 m Vs^{-1}. However, EIS measurements were obtained using a frequency domain in the range 10^5–10^{-2} Hz at E_{ocp} by overlaying alternating current (AC) signal of 10 mV.

2.5. UV–visible spectroscopy

UV-visible spectrometry was carried out using a Jenway UV-visible spectrophotometer (67 series); the UV-visible experiments were made before and after immersion of carbon steel for 48 h in corrosive solution in absence and presence of optimum concentrations of each inhibitor

2.6.Computational. details

The details of DFT calculations, Metropolis Monte Carlo (MC) simulations and their software employed have already been discussed [29]. Protonation of the BHMB and HMPB in the whole pH range from 0–14 were predicted using ACD/Percepta™-14 Software (ACD/Labs, Toronto, Canada) Licensed to KFUPM, 2018.

3. Results and discussion

3.1. Effect of both BHMB and HMPB concentration

3.1.1. Weight loss measurements

The two organic compounds (BHMB and HMPB) were investigated in a range of concentration 10^{-3} to 10^{-6} M. The limits of this interval is determined by their solubility (for maximum concentration) and the protective effect reached (for the minimum concentration).

The impact of BHMB and HMPB on the corrosion of carbon steel (CS) was analyzed gravimetrically after 6 h of the immersion period at 298 K. The results are presented in Table 1. The next formulas 1 and 2 are applied to establish of the corrosion rate (Rate) and the effectiveness of the protection (η_{wl}(%)), respectively.

$$Rate = \frac{\Delta m}{St} \tag{1}$$

$$\eta_{wl}(\%) = \left(1 - \frac{Rate}{Rate^{\circ}}\right) \times 100 \tag{2}$$

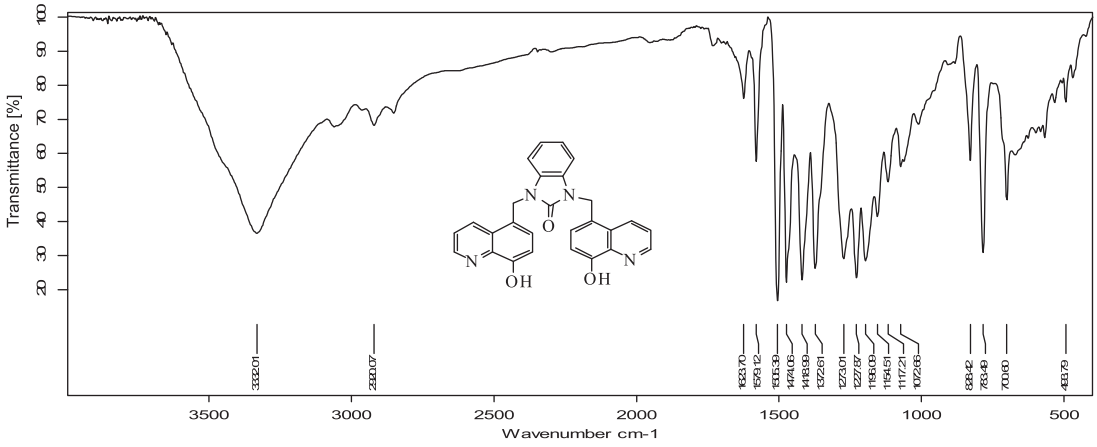

Fig. 4. IR spectrum of 1,3-bis((8-hydroxyquinolin-5-yl)methyl) − 1H-benzimidazol-2(3H)-one (BHMB).

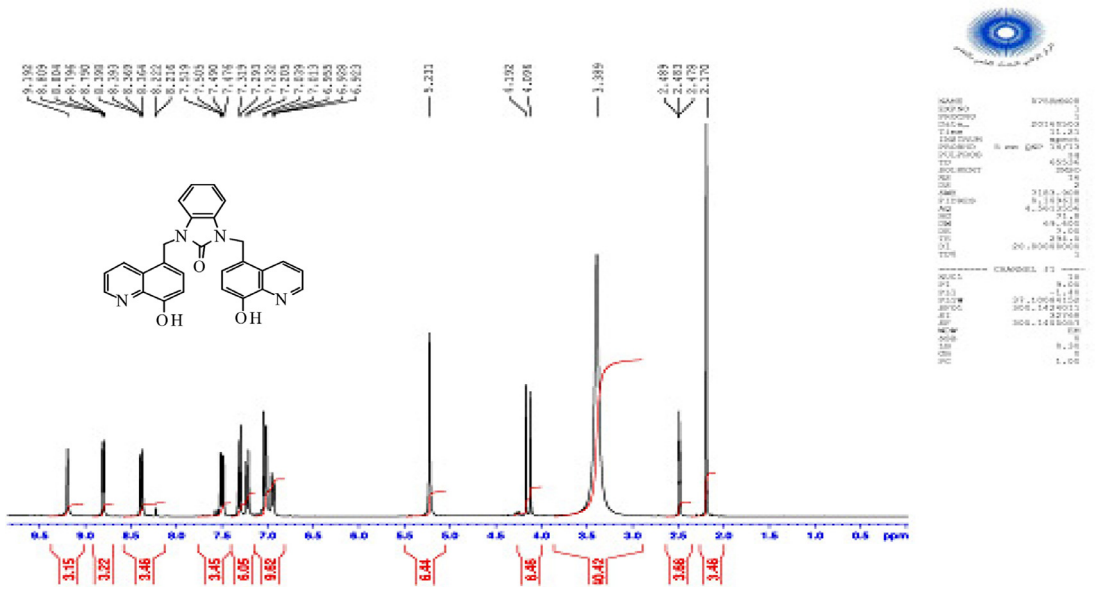

Fig. 5. ^{1}H NMR spectrum of 1,3-bis((8-hydroxyquinolin-5-yl)methyl) – 1H-benzimidazol-2(3H)-one (BHMB) (in DMSO-d6).

Where Δm (mg) is the mass loss, S (cm^2) the total surface of the steel sample (cm^2), t (h) is the immersion time, (*Rate* and *Rate*$^{\circ}$) are the corrosion rates of carbon steel with and without of quinoline derivatives, respectively.

Table 1 regroups the obtained gravimetric data of CS in 1 M HCl with and without the addition of diverse concentrations of benzimidazol-2-ones substituted 8-hydroxy-quinoline derivatives tested. We noted from the results of this table, that the corrosion rate (*Rate*) of CS decreases when the concentration of BHMB or HMPB increases. The protective effect is more obvious for BHMB reach 91% at 10^{-3} M. It is widely known that the organic molecules acts by adsorption (physisorptions or /and chemisorption) at the CS/electrolyte interface [30]. So, the adsorption of BHMB and HMPB under the neutral form might happen because of the formation of links with the d-orbital of metal atoms, involving the displacement of water molecules from the metal surface, and the lone pairs exist on the N and O atoms and π-orbitals in the benzimidazole and quinoline rings act by blocking the active sites of acid attack, reflecting a reduce of corrosion rate [31].

Table 1
Gravimetric data for carbon steel in 1 M HCl at various concentrations of BHMB and HMPB.

Medium	Conc. (M)	*Rate* (mg cm^{-2} h^{-1})	η_{wl} (%)
1 M HCl	0	1.740	——
BHMB	10^{-3}	0.160	90.8
	10^{-4}	0.224	87.1
	10^{-5}	0.311	82.1
	10^{-6}	0.435	75.0
HMPB	10^{-3}	0.213	87.7
	10^{-4}	0.341	80.4
	10^{-5}	0.418	76.0
	10^{-6}	0.497	71.4

Furthermore, by virtue of the availability of heteroatoms on the two molecules, BHMP and HMPB can quickly ionize to generate cations in 1 M HCl and that adsorb later at the metal interfaces by means of adsorbed chloride ions.

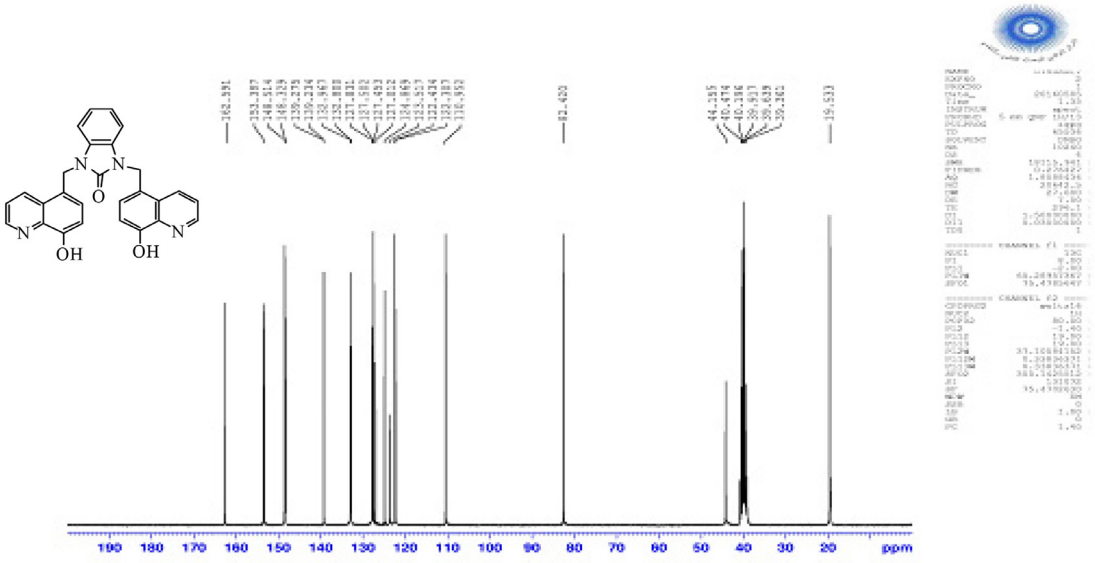

Fig. 6. ^{13}C NMR spectrum of 1,3-bis((8-hydroxyquinolin-5-yl)methyl) – 1H-benzimidazol-2(3H)-one (BHMB) (in DMSO-d6).

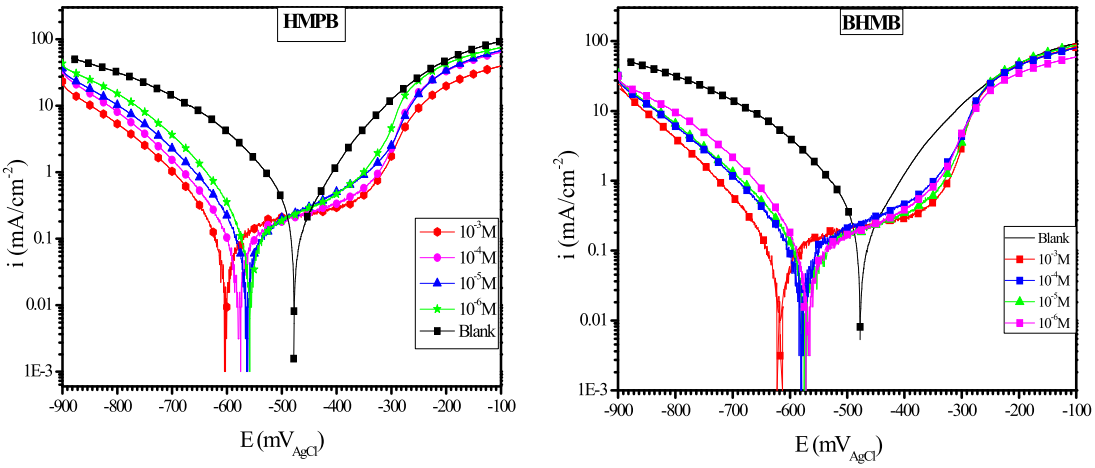

Fig. 7. Tafel plots for CS in 1 M HCl without and with HMPB and BHMB.

The high performance ability for 1,3-bis((8-hydroxyquinolin-5-yl) methyl) − 1H-benzimidazol-2(3H)-one (BHMB) compared with 1-((8-hydroxyquinolin-5-yl)methyl) − 3-(prop-1-en-2-yl) − 1H-benzimidazol-2(3H)-one(HMPB) was attributed to the presence of two groups 5-methy8-hydroxyquinoline in 1 and 3 position (electron donor by inductive effect (+ I)), more of *N, O* atoms, heterocyclic and aromatic rings enriches the electron density on the benzimidazolone BHMQ, whereas the HMPB contains only a single group of 5-methy8-hydroxyquinoline, this justified the observed difference.

3.1.2. Polarization results

Tafel plots for carbon steel in 1 M HCl with different concentrations of both BHMB and HMPB are illustrated in Fig. 7.

The values of current densities extrapolated from Tafel plots were used to determine the performance ability (η_p %), the latter was determined by applying the below Eq. (3):

$$\eta_p(\%) = \frac{i^{\circ}_{corr} - i_{corr}}{i^{\circ}_{corr}} \times 100 = \theta \times 100 \quad (3)$$

Where i°_{corr} and i_{corr} are the corrosion current density values for steel electrode without and with the quinoline derivative, respectively, and θ is the fraction of surface coverage which will be later used.

The extrapolated corrosion parameters including corrosion potential (E_{corr}), corrosion current density (i_{corr}), the performance ability (η_p (%)) and Tafel cathodic constant (β_c) were listed in Table 2.

Based on the results obtained, it is clear that the addition of both BHMB and HMPB cause the decrease in both anodic and cathodic densities, this decrease is relative with the concentrations of BHMB and HMPB (Fig. 7). Also, the presence of the synthesized compounds shifted the E_{corr} value toward the negative direction in comparison to the blank solution; these results reveal that the HMPB and BHMB restrict the metal dissolution process and H_2 gas evolution attributable to anodic and cathodic reactions respectively. In addition, the increase of protective effect with inhibitor concentration reveals that BHMB and HMPB compounds react by adsorption on the metallic surface [32]. According to the literature [33], if the difference in E_{corr} between inhibited systems with respect to uninhibited is greater than 85 mV, the inhibitor can be considered as a cathodic or anodic type, but if the difference in E_{corr} is less than 85 mV, the inhibitor can be classified as mixed type. In our case, the obtained displacement range was 87–141 mV on the cathodic part, which means that BHMB and HMPB are cathodic inhibitors. However, the addition of benzimaidazole-2-one derivatives leads to a change in cathodic Tafel slopes (β_c) indicating a change of the mechanism of cathodic hydrogen evolution also, reveals that both BHMP and HMPB strongly inhibit the corrosion process of steel [34] in the anodic domain. The current density remains constant in the potential region of 550–300 mV. The current plateau can be explained by the formation of a film of inhibitor protective character to the metal surface [35]. For potential more positive than −300 mV_{AgCl}, the steel dissolution rate increased rapidly even in the presence of BHMB and HMPB. This potential is generally known by desorption potential [36], this can be elucidated by desorption of inhibitors molecules (BHMB and HMPB), which increases the active surface and consequently the increase of the rate of the corrosion. From the structure of benzimaidazole-2-one derivatives, which include heteroatoms with a lone pair of electrons such as N and O atoms in the quinoline, benzimidazol rings, can be facilitated the formation of Fe(II)-BHMB or Fe(II)-HMPB complex compound and thus changes the dissolution mechanism of iron. Both BHMB and HMPB compounds show η_p (%) higher in value compared to that obtained through gravimetric measurement. The difference obtained between both values could be due to the immersion time. But, potentiodynamic polarization measurements confirm the better performance of BHMB compared to HMPB.

Table 2
Electrochemical parameters of CS before and after HMPB and BHMB compounds addition in 1 M HCl.

Medium	Conc. (M)	i_{corr} (μA cm^2)	-E_{corr} (mV_{AgCl})	-β_c (mV/dec)	η_p(%)	θ
Blank	0	900	475.1	160.1	——	——
BHMB	10^{-3}	78.7	616.2	100.5	91.2	0.912
	10^{-4}	84.1	576.1	99.2	90.6	0.906
	10^{-5}	106.0	574.0	105.4	88.2	0.882
	10^{-6}	119.8	570.6	90.7	86.7	0.867
HMPB	10^{-3}	92.5	600.8	99.4	89.7	0.897
	10^{-4}	110.9	570.0	96.3	87.7	0.877
	10^{-5}	135.1	562.8	90.1	85.0	0.850
	10^{-6}	165.6	564.5	100.2	81.6	0.816

3.1.3. Electrochemical impedance spectroscopy (EIS)

To estimate the rate of performance ability, characterize the various processes of corrosion and study the reaction mechanisms in the electrochemical interface, EIS was utilized. Fig. 8 illustrates the Nyquist plots for CS obtained in 1 M HCl solution containing diverse concentrations of benzimidazol-2-one derivatives (BHMB and HMPB), the addition of BHMB and HMPB causes an increase in the capacitive loops than the reference solution, considering the shape of the impedance diagram, we can say that their size depends on both structure and concentration of inhibitor, the Nyquist representations spectra consisting one single capacitive loop slightly depressed. This kind of diagram exhibit generally that the charge transfer controls corrosion reaction on inhomogeneous of electrode surface [37].

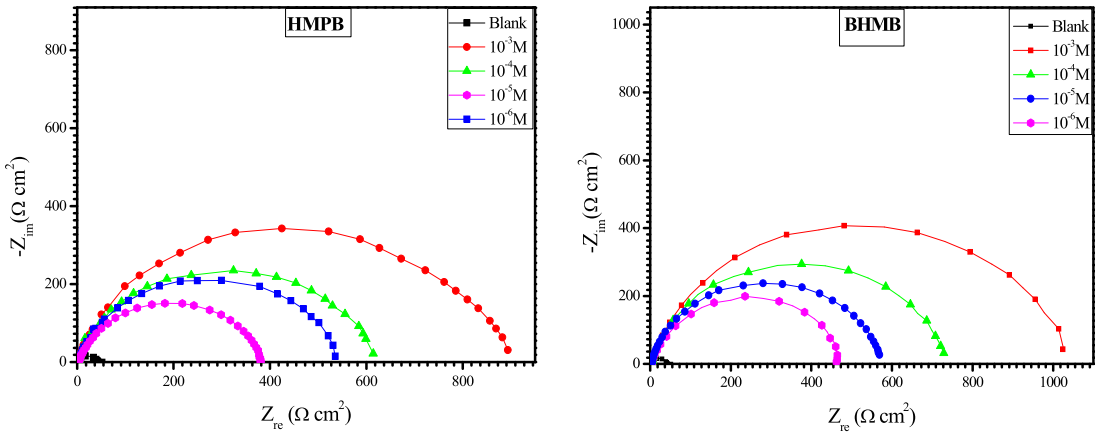

Fig. 8. Nyquist plots of CS in electrolyte only and with various concentrations of BHMB and HMPB.

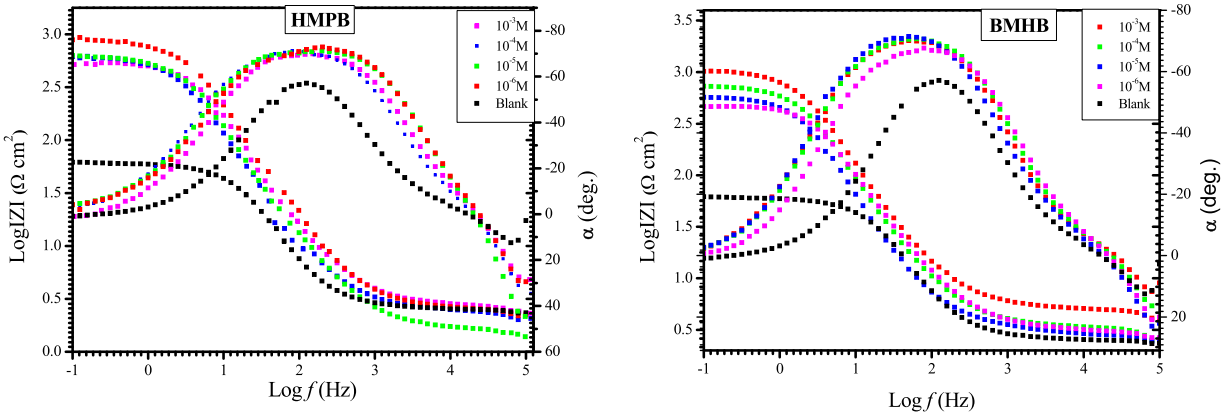

Fig. 9. Bode plots for CS in electrolyte only and with diver's concentrations of both inhibitors at 298 K.

Fig. 9. provide the Bode plots (log |Z| against log (*f*) and (phase angle (α) vs.log (*f*)) curves for CS in blank solution containing diverse concentrations of benzimidazol-2-one derivatives, the analysis of these figures show three different regions, in the higher frequency part, the log |Z| values tend to become zero and the phase angle values approaching toward 0°, these are the responses to resistive behavior and attributed to the electrolyte resistance. For intermediate frequency regions, there is a linear correlation across log |Z| versus log *f*, with slope less than −1 and the phase angle inferior to −90° Ideally, a pure capacitor's characteristics would lead to slope of −1 and a phase angle of −90°, however the deviations obtained account for the deviation from an ideal capacitive response could be related to the slowing down of the rate of dissolution with time [38], Finally at the low frequency region, the resistive behaviour of the electrode increases, and log |Z| becomes independent of frequency [39].

All the experimental data are fitted (typical example Fig. 11) utilizing the equivalent circuit presented in Fig. 10, the inventive circuit includes such elements as: R_p which is defined by the polarization resistance, R_s stands for the resistance of solution between working and platinum electrode and CPE corresponding to the constant phase element, the latter introduced in order to make up for the inhomogeneity in a system and defined by (4) [40]:

$$Z_{CPE} = A^{-1}(iw)^{-n} \tag{4}$$

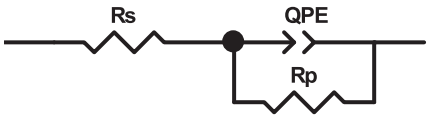

Fig. 10. equivalent circuit employed for fitting of all EIS curves.

Where *A* is the CPE constant in ($\Omega^{-1}s^{n}cm^{-2}$), *n* is the CPE exponent determining the phase shift (ranges from 0 to 1), $i^2 = 1$ is an imaginary number and *w* is the angular frequency in (rad s^{-1}) ($w = 2\pi f$, where f is the frequency),

The double layer usually (C_{dl}) behaves as a constant-phase element (CPE) when the value of n is equal to unity, the C_{dl} values are obtained by exploiting the next formula (5) [41]:

$$C_{dl} = (A_d R_p^{1-n})^{1/n} \tag{5}$$

The relaxation time parameter (τ_d) is defined as the time necessary to reset the charge distribution after an electric perturbation and expressed as:

$$\tau_d = C_{dl} R_p \tag{6}$$

The term of performance ability (η_{EIS}) is expressed by the following Eq. (7):

$$\eta_{EIS}(\%) = \left(1 - \frac{R_p^{\circ}}{R_p}\right) \times 100 \tag{7}$$

Where R_p° and R_p are the polarization resistance values in the absence and presence of synthesized benzimidazol-2-ones substituted 8-hydroxyquinoline derivatives, respectively.

The most parameters cited previously are inserted in Table 3. Analysis of the impedance data reveals that the polarization resistance value (R_p) increases more in presence of synthesized benzimidazol-2-ones substituted 8-hydroxyquinoline derivatives that in their absence and affected a value of about 1.027 KΩ cm^2 in the case of BHMB. The higher value of R_p is attributed a slower system of corrosion caused by a decrease in the active surface necessary for the corrosion reaction. The values of R_p respect the sequence of BHMB > HMPB and the values of *A*

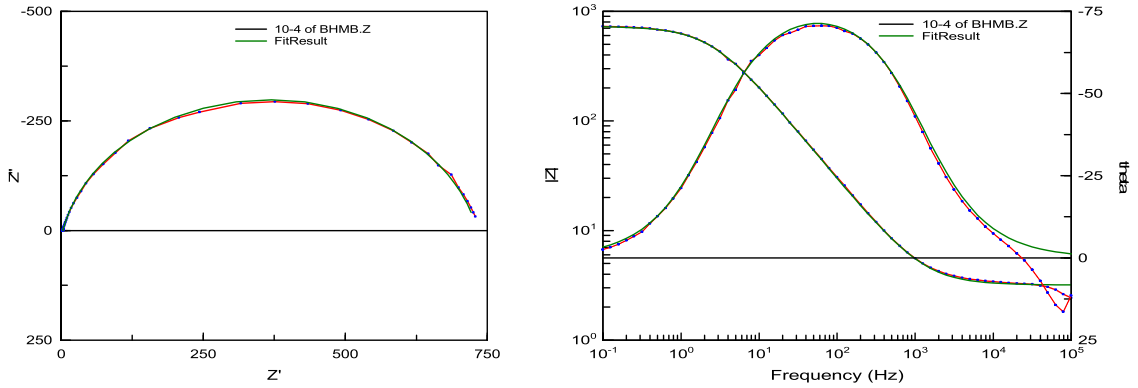

Fig. 11. Typical example of EIS and Bode plots simulated in 1 M HCl in presence 10^{-4} M of BMHB.

follow the order of HMPB < BHMB, leading to the performance ability order: BHMB > HMPB, a significant reduction was observed in the value of the C_{dl} with the increasing of concentration of inhibitor. For example, their value decreases from 339.89 (μF cm^{-2}) in the electrolyte to 97.40 (μF cm^{-2}) in the case of 10^{-3} M of BHMB which means that a reduction in local dielectric constant and/or a raise in the thickness of the electrical double layer. However, it is clear that the n values raise from 0.820 to 0.890 with inhibitor concentration, suggesting the reduction of the surface heterogeneity in consequence of the adsorption of benzimidazol-2-ones ions on CS surface by creating a uniform protective film [42]. In addition, the τ_d values rise with quinoline derivative concentrations suggest that the time of adsorption process turned higher, which causes a slow adsorption reaction. BMHB has higher value of τ_d, which indicates that BMHB corresponds to the slowest adsorption process [43]. Thus, ac impedance study confirms the priority in term of protection ability of BHMB in comparison with HMPB, but in general the both organic compounds exhibit a good protection ability effect for CS in acidic media, this result is in good agreement with the two previous techniques.

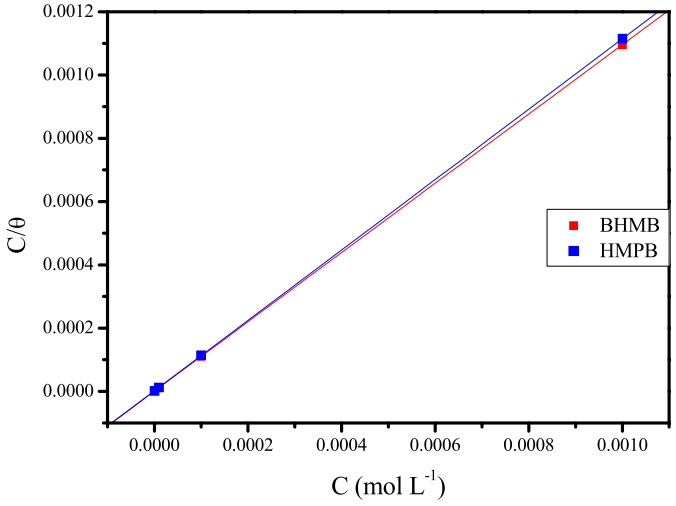

Fig. 12. Langmuir adsorption isotherm for both inhibitors (BHMB or HMPB + 1 M HCl).

3.1.4. Adsorption isotherm

As is well known, the organic compounds interact chemically, physically or by complexation with metal ions. The adsorption isotherm contribute to the study of adsorption process. It is well documented that the adsorption depends on factors like metal, chemical specie and nature of the corrosive medium. In order to determine the appropriate adsorption isotherm, many isotherms were tested, but the use of the Langmuir isotherm provides a best straight-line fit. In this case, the fraction of surface coverage (θ) for different concentration of BHMB and HMPB in HCl 1 M at 298 K has been calculated from the values of η_p obtained by polarization measurements following the ratio η_p (%)/100.

For BHMB and HMPB, the plots of $C_{inh}\ \theta^{-1}$ versus C_{inh} presents a linear line Fig. 12) with correlation coefficient (R^2) equal to unity suggesting that the adsorption of BHMB and HMPB on the CS surface is well obey to the Langmuir adsorption isotherm [44], which follows the relation ((8) mentioned below.

$$\frac{C_{inh}}{\theta} = C_{inh} + \frac{1}{K_{ads}} \tag{8}$$

Where K_{ads} is the adsorptive equilibrium constant; their values were estimated via intercept of Langmuir isotherm plot and employed thereafter to determine the standard Gibbs energy of adsorption ΔG°_{ads} according to the expression (9) [45]:

$$\Delta G^{\circ}_{ads} = -RTLn(55.5K_{ads}) \tag{9}$$

In this expression 55.5 value correspond to the molarity of water; T is the temperature of study (298 K) and R is the universal gas constant (8.3143 J K^{-1}mole^{-1}).

The obtained values of K_{ads} for BHMB and HMPB are 25.829 × 10^5

Table 3
EIS data of CS in 1 M HCl without and with diver's concentrations of BHMB and HMPB.

Medium	[C] (M)	R_s (Ω cm^2)	R_p (Ω cm^2)	CPE 10^6 A (Ω^{-1} S^n cm^2)	n	10^6 C_{dl} (Fcm^{-2})	τ_d (ms)	η_{EIS} (%)
1 M HCl	00	2.439 ± 0.03	56.9 ± 0.04	339.89 ± 0.006	0.800 ± 0.002	126.75	07.21	——
BMHB	10^{-3}	2.778 ± 0.04	1027.1 ± 0.02	97.408 ± 0.001	0.862 ± 0.003	067.38	69.20	94.5
	10^{-4}	3.163 ± 0.03	730.2 ± 0.08	127.89 ± 0.004	0.868 ± 0.003	089.17	65.09	92.2
	10^{-5}	2.881 ± 0.02	570.5 ± 0.07	150.82 ± 0.005	0.885 ± 0.001	109.65	62.55	90.0
	10^{-6}	3.039 ± 0.05	468.0 ± 0.03	170.02 ± 0.003	0.890 ± 0.002	124.34	58.19	87.8
HMPB	10^{-3}	2.456 ± 0.06	890.1 ± 0.08	100.74 ± 0.006	0.849 ± 0.004	065.60	58.39	93.6
	10^{-4}	2.514 ± 0.03	613.2 ± 0.01	129.12 ± 0.003	0.845 ± 0.003	081.08	49.72	90.7
	10^{-5}	2.693 ± 0.04	530.2 ± 0.03	135.07 ± 0.005	0.849 ± 0.002	084.51	44.80	89.3
	10^{-6}	2.936 ± 0.02	378.1 ± 0.06	146.20 ± 0.002	0.852 ± 0.001	088.41	33.42	84.9

M^{-1} and 9.122×10^5 M^{-1}, respectively; corresponding to the values for ΔG°_{ads} of -46.531 kJ mole^{-1} and -43.952 kJ mole^{-1}, respectively. The high values of K_{ads} indicate that the studied compounds have a high affinity to adsorb on CS surface and confirms the performance of BHMB and HMPB as excellent corrosion inhibitors. However, the negative values of ΔG°_{ads} confirming the extensive adsorption of BHMB and HMPB [46].

According to the literature [47], for a physisorption mechanism, the ΔG°_{ads} values are equal or less negative than -20 kJ mole^{-1}, whereas ΔG°_{ads} values of over -40 kJ mole^{-1} or more negative corresponds to chemisorption mechanism. Based on the data obtained, the interaction of both BHMB and HMPB with the surface of CS in 1 M HCl were chemisorption in nature.

3.2. Influence of temperature

3.2.1. Corrosion kinetic and thermodynamic parameters studies

The temperature has a significant effect on the corrosion rate and behavior of molecules or ions in a given media, the increase of the temperature would promote desorption of the inhibitor molecules and would lead to a fast dissolution of organic compounds or the formed complexes, thereby causing a weakening of the corrosion resistance of the steel. To determine the effect of this variable on the performance ability of the both BHMP and HMPB molecules on the CS, EIS measurement ware taken at various temperatures. The Nyquist plots for CS corrosion without and with BHMP and HMPB at 10^{-3} M in the temperature range of 298–328 K are shown in Fig. 13(A). The impedance spectra obtained in the studied medium with and without the benzimidazol-2-one derivatives are made of one capacitive loop, while their diameters decrease with increasing temperature and correspond to one time constant, as illustrated in bode-phase plots (Fig. 13(B)). On the other hand, the impedance spectra were fitted utilizing the same equivalent electrical circuit proposed previously. As a typical example, the Nyquist and Bode curves of both experimental and fitted for CS in the electrolyte (1 M HCl) containing 10^{-3} M of HMPB at 328 K are illustrated in Fig. 14. And the corresponding parameters were summarized in Table 4. The analysis of Table 4 shows that the R_p values decrease with increasing temperature in electrolyte and after addition of both synthesized compounds, which can be related to desorption of inhibitor molecules from metal surface releasing larger surface area to electrolyte [42,48]. The decrease of $\boldsymbol{n}$ value with temperature increase suggests that the surface inhomogeneity increases and this can be linked also with the increase in the rate of corrosion [49]. However, the C_{dl} values in the presence of benzimidazol-2-one derivatives at high temperatures are lower when compared to those in 1 M HCl, and their values increased with temperature increase. This is attributed as an evidence for a reduction of the role of adsorption resulting in the substitution of BHMP and HMPB molecules with H_2O molecules. Moreover, similar tendency was found for $\boldsymbol{A}$ values for all temperatures studied both in uninhibited and inhibited solutions. Despite these conditions, the BMHB and HMPB compounds preserve their very good protective effect and more especially BMHB.

The obtained data are used subsequently to estimate the thermodynamic and activation parameters. For this purpose, the corrosion current density value (i^*_{corr}) without and with BHMB and HMPB at various temperatures was determined from R_p using Eq. (10) [50] and their values are given in Table 4.

$$i^*_{corr} = RT\,(zFR_p)^{-1} \tag{10}$$

where z corresponds to the valence of iron (z = 2) and F represents the Faraday constant (F = 96 485 C).

The activation parameters of the investigated system were estimated using the Arrhenius' Eq. (11) [51]:

$$i^*_{corr} = A \exp\left(\frac{-E_a}{RT}\right) \tag{11}$$

Where A is defined as a constant for each chemical reaction and E_a represent the activation energy. Fig. 15 represents the Arrhenius plots of Lni^*_{corr} against 10^3/T in both uninhibited and inhibited solutions, the linear regression of Arrhenius plots provide the value of activation energy.

Inspection of Table 5 reveals that the values of E_a in the presence of BHMB and HMPB are superior than that of blank solution; the increase in E_a indicates that the adsorption mechanism of synthesized compounds in 1 M HCl is of physisorption character [52]. However, Fan Zhang opined that the small increase in activation energy could not be regarded as decisive because of the competitive adsorption with water whose removal from the surface needs an extra activation energy [53].

An alternative form of the corrosion current density is used out this time to calculate enthalpy (ΔH_a) and entropy (ΔS_a) of activation (12) [54].

$$i^*_{corr} = \frac{RT}{Nh} \exp\left(\frac{\Delta S_a}{R}\right) \exp\left(-\frac{\Delta H_a}{RT}\right) \tag{12}$$

Where h recognized by the Plank's constant (6.6261×10^{-34} J s) and N represent the Avogadro's number (6.022 10 ^{23} mol − 1).

Fig. 16 exhibits the variation of $Ln\frac{i^*_{corr}}{T}$ against of 10^3/T, three straight lines were obtained with the slope of (-ΔH_a/ R) and intercept (Ln(R/Nh) + ΔS_a/R), from which the values of ΔH_a and ΔS_a have been obtained and summarized in Table 5.

Inspection of Table 5 shows that the values of ΔH_a in the presence of HMPB and BHMP are superior to that of blank solution. The positive sign of ΔH_a is generally attributed to the endothermic process, which indicate that the dissolution reaction of CS is very slow. From published studies [55], it is important to note that the values of ΔH_a less than or equal to 41 kJ/mole are attributable to the electrostatic interactions between active sites of the metal and inhibitory particles (physisorption), while the values of ΔH_a around 100 kJ/mole or more positive are relative to the charge sharing between inhibitor and metallic surfaces (chemisorption), In our case, the calculated values of ΔH_a for BMHB, and HMPB are 32.758 and 41.635 KJ/mole respectively, suggesting that the mode adsorption of the both inhibitors on CS is physisorption.

The adsorption of BHMB or HMPB molecules is always accompanied by water desorption and their competition between them leads to certain disorder of the system, resulting in a variation of the entropy. So, the negative values of ΔS_a of both inhibitors BMHQ and HMHQ reveals that the arrangement created by the adsorption of BMHQ and HMHQ molecules is greater than the disorder caused by solvent (H_2O) desorption. On the other hand, the less negative values of ΔS_a for HMPB in comparison with uninhibited medium is attributed to the creation of an ordered stable layer of HMPB molecules on the CS surface [56,57].

3.3. UV − Visible spectroscopy

To probe whether the examined molecules can form complexes with iron ions, UV–Visible spectra of HMPB and BHMP at 10^{-3} M were obtained after 48 h of CS immersion in the electrolyte as presented in Fig. 17.

The absorbance spectra of HMPB prior the immersion of the steel exhibit two absorption peaks at 206 nm and 228 nm (Fig. 17(A)), which are due π-π* transitions [58], also another band at around 270 nm corresponding to the n-π* transitions. But after immersion, it emerged that there is a marked difference compared to the spectrum before immersion, for example, the peak initially at 273 nm has been shifted to a higher value at 333 nm and revealed a significant enhancement of absorbance.

It should be noted that there is no meaningful difference in the bulk form of the spectra in the range 200–300 nm between the UV–visible spectra of BHMB prior and after CS immersion (Fig. 17(B)). Furthermore, BHMB after immersion showed the appearance of a peak at 330 nm.

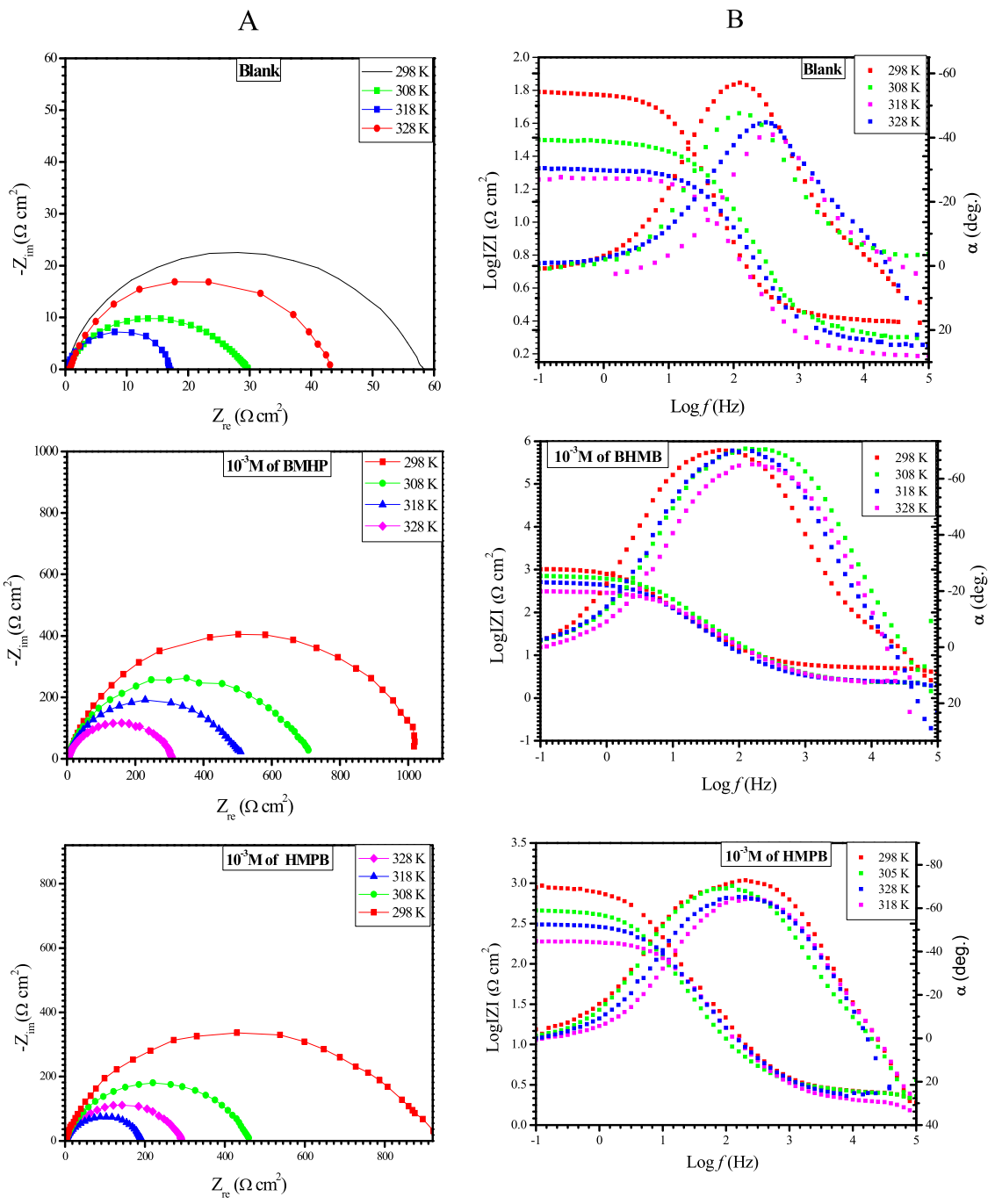

Fig. 13. Nyquist (A) and corresponding Bode-phase curves (B) for CS in the electrolyte (1 M HCl) solution without and with 10^{-3} M of HMPB and BHMB at diverse temperatures.

The noticeable variation in the absorbance spectrum after the immersion of CS in the presence of benzimidazol-2-one justified the formation of the complex between the iron cations and synthesized benzimidazol-2-ones substituted 8-hydroxyquinoline molecules.

3.4. Computational studies

Prediction of the protonation of HMPB and BHMB versus pH was carried out to ascertain which form of the molecules are predominant in 1 M HCl (pH = 0) using ACD/PerceptaTM-14 Software. The results obtained for the protonation predictions for the two studied molecules are shown in Figs. 18 and 19 respectively. The results indicates that the neutral form of the molecules were dominant in the pH of interest (pH = 0) in the presence of other protonated species. Therefore, we adopted the neutral form of the two molecules for DFT and Monte Carlo simulations.

DFT methodology was used to compute the reactive sites of BHMB and HMPB to understand the regions in the molecules where interaction with steel surface can occur. Overall, HOMO and LUMO orbitals indicate the molecular sites which can yield or accept electron, respectively. A large HOMO orbital corresponds to a molecule that can easily gives electron to unoccupied d-orbital of a metal atom. On the other hand, a large LUMO orbital attributes to a molecule which can easily accept electrons from a d-orbital metal atom. The optimized geometry, HOMO and LUMO orbitals of HMPB and BHMB molecules utilizing DFT model chemistry are illustrated in Fig. 20. The result from the figure

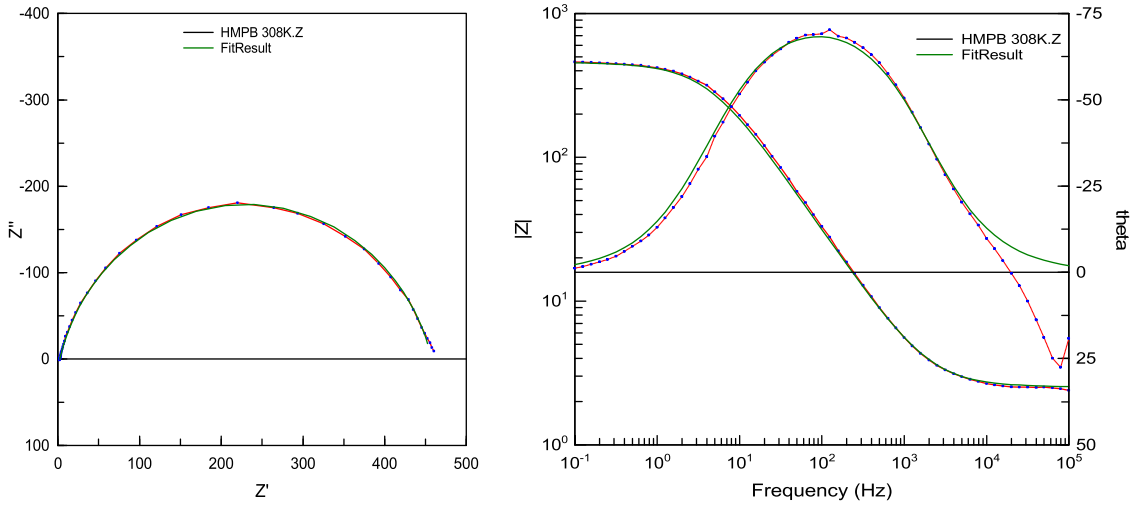

Fig. 14. Typical example of EIS and Bode curves simulated in 1 M HCl + 10^{-3} M of HMPB at 308 K.

Table 4
Electrochemical parameters for CS in electrolyte (1 M HCl) without and with 10^{-3} M of HMPB and BHMB at diverse temperatures.

Medium	T (K)	R_s (Ω cm^2)	R_p (Ω cm^2)	CPE 10^6A (Ω^{-1} S^n cm^2)	n	10^6 C_{dl} (Fcm^{-2})	τ_d (ms)	i^*_{corr} (μA/cm^2)	η_{EIS} (%)
1 M HCl	298	2.439 ± 0.03	56.90 ± 0.04	339.89 ± 0.006	0.800 ± 0.002	126.75	7.21	225.64	——
	308	2.026 ± 0.03	43.12 ± 0.06	360.26 ± 0.009	0.800 ± 0.006	127.18	5.48	307.74	——
	318	2.016 ± 0.04	28.67 ± 0.03	401.92 ± 0.008	0.798 ± 0.003	129.85	3.72	477.88	——
	328	1.616 ± 0.08	18.91 ± 0.07	443.21 ± 0.009	0.797 ± 0.008	131.12	2.38	747.70	——
BMHB	298	2.778 ± 0.04	1027.1 ± 0.02	97.408 ± 0.001	0.862 ± 0.003	67.38	69.20	12.50	94.5
	308	2.026 ± 0.04	705.0 ± 0.02	108.21 ± 0.001	0.860 ± 0.001	71.10	49.78	18.81	93.9
	318	2.326 ± 0.02	498.2 ± 0.01	126.10 ± 0.003	0.854 ± 0.004	78.59	39.23	27.44	94.2
	328	2.399 ± 0.03	299.3 ± 0.03	159.70 ± 0.002	0.852 ± 0.005	93.71	28.04	47.21	93.7
HMPB	298	2.456 ± 0.06	890.1 ± 0.08	100.74 ± 0.006	0.849 ± 0.004	65.60	58.39	14.42	93.6
	308	2.523 ± 0.06	455.2 ± 0.07	125.01 ± 0.004	0.848 ± 0.002	74.78	34.04	29.15	90.5
	318	1.815 ± 0.04	290.5 ± 0.05	139.01 ± 0.003	0.839 ± 0.005	75.08	21.81	47.16	90.1
	328	1.914 ± 0.05	188.2 ± 0.06	165.08 ± 0.003	0.832 ± 0.003	81.89	15.41	75.08	89.9

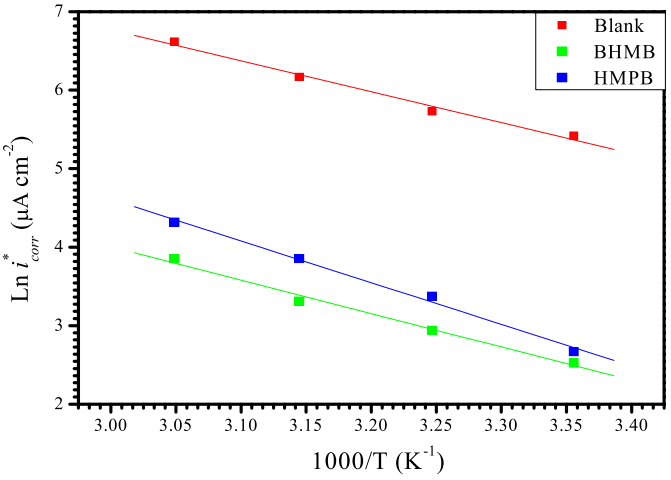

Fig. 15. Arrhenius plots for CS obtained in 1 M HCl only and with 10^{-3} M of both HMPB and BHMB.

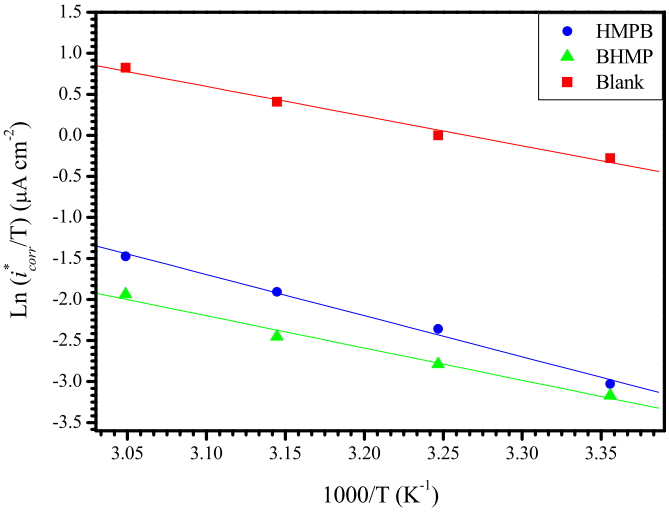

Fig. 16. Transition state plot for CS obtained in 1 M HCl only and with 10^{-3} M of synthesized compounds.

Table 5
Thermodynamic Activation parameters for CS in 1 M HCl without and with 10^{-3} M of various synthesized compounds.

Medium	R^2	E_a (KJ $mole^{-1}$)	ΔH_a (KJ $mole^{-1}$)	$-\Delta S_a$ (J $mole^{-1}$ K^{-1})
Blank	0.99	32.69	30.19	99.29
BHMP	0.99	35.32	32.76	114.37
HMPB	0.99	44.23	41.63	82.58

indicates that the HOMO for BHMB is localized on the benzimidazole ring and on one of the 8-hydroxquinoline ring. These two hetero rings are the main active sites that donate electron density to the steel surface during inhibition of steel corrosion. On the other hand, the HOMO for HMPB is located only on the benzimidazole ring. The location of the HOMO orbitals for BHMB on two rings indicate why the interaction of BHMB is stronger with the steel surface than with HMPB. The LUMO

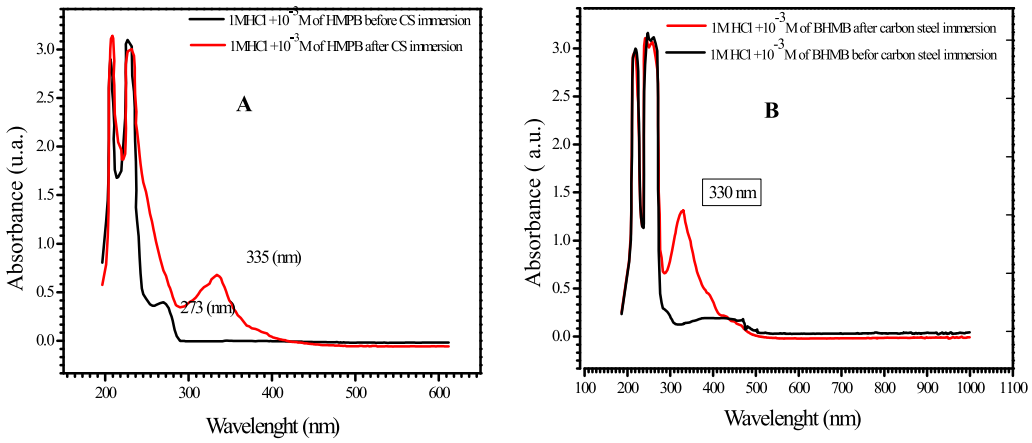

Fig. 17. UV − visible spectra of 1 M HCl medium include 10^{-3} M of HMPB and BHMB before (black color) and after (red color) 48 h of carbon steel immersion, (A) HMPB and (B) BHMB.

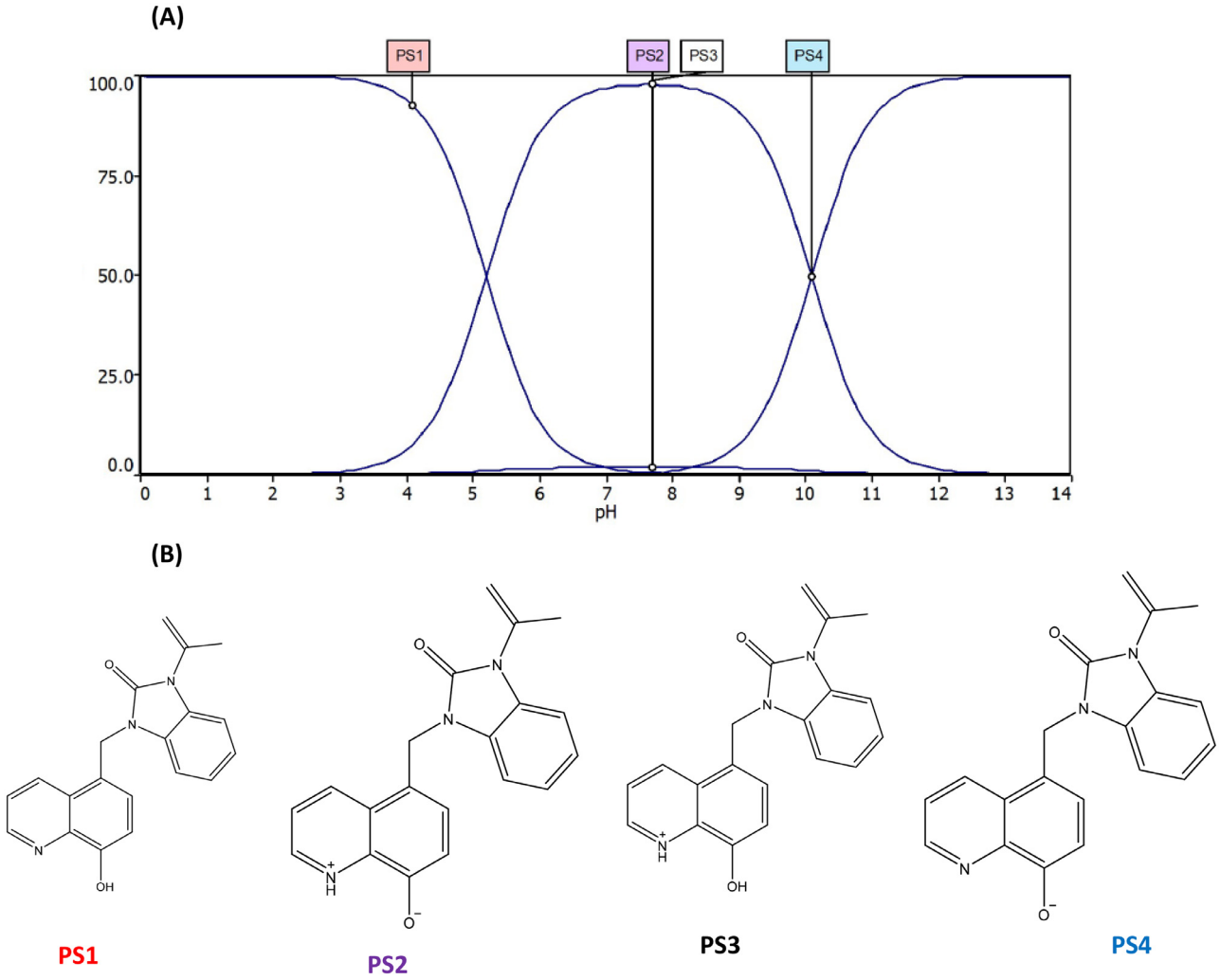

Fig. 18. (A) The curve of protonated state vs pH of HMPB predicted using ACD/LABS Software and (B) The molecular structures corresponding to the four states PS1-PS4.

orbitals for both molecules are located on the 8-hydroxquinoline ring. Thus, the reactivity of BHMB and HMPB towards the steel surface is controlled by the HOMO orbital.

To understand further the interaction of the investigated molecules with steel surface, Monte Carlo simulation utilizing a simulated annealing procedure was carried out. This methodology has been adopted previously by us to compute the adsorption energies of organic molecules on Fe surface [59,60]. Fig. 21 shows (a) snapshot of the stable equilibrium configuration of BHMB adsorption on Fe (110) surface and (b) snapshot of the stable equilibrium configuration of HMPB adsorption on Fe (110) surface. Table 6 outlines the output of the data obtained employing Monte Carlo simulations. As as reflected in Fig. 21(a)

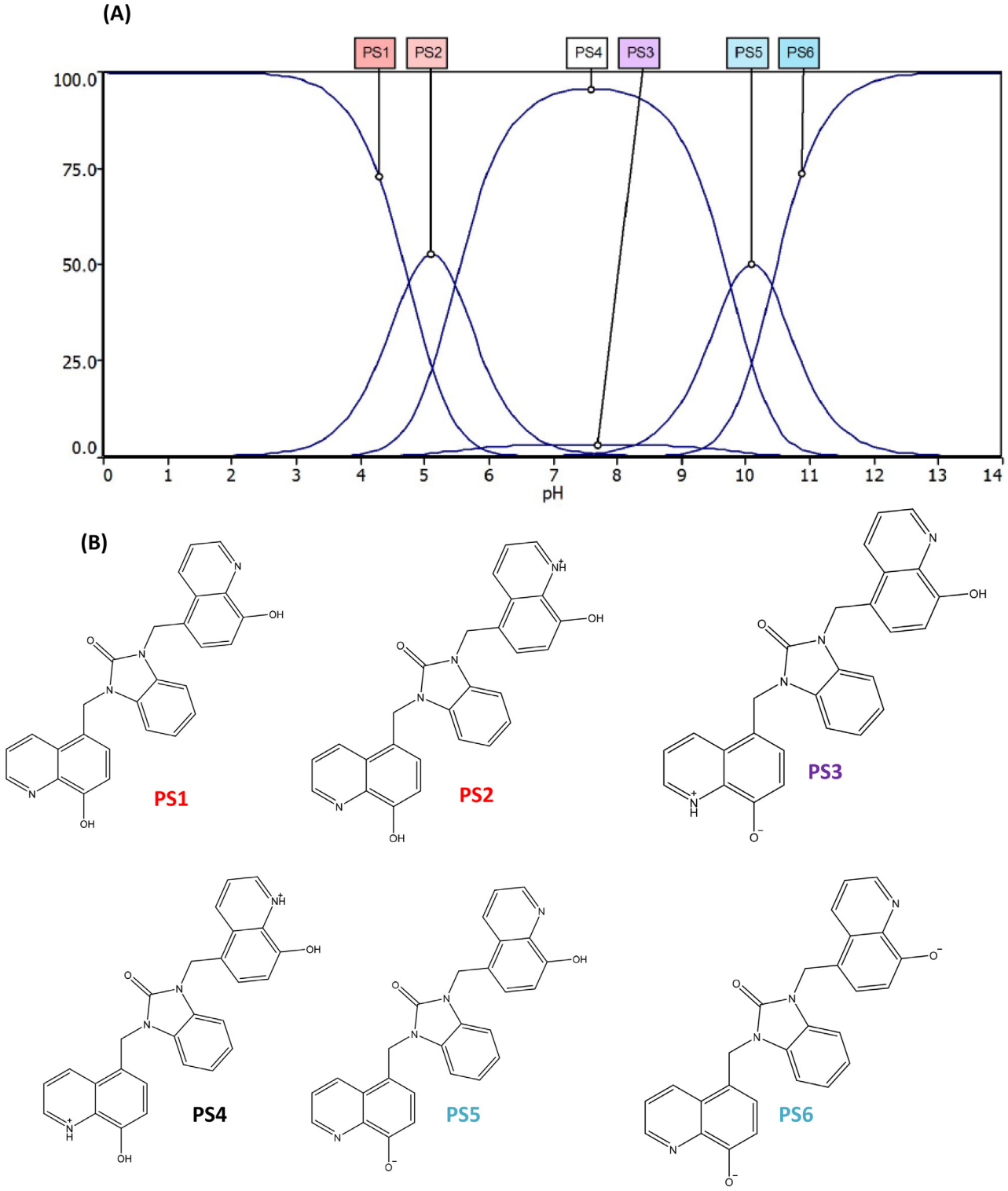

Fig. 19. (A) The curve of protonated state vs pH of BHMB predicted using ACD/LABS Software and (B) The molecular structures corresponding to the six states PS1-PS6.

and (b) BHMB and HMPB molecules are adsorbed in a way parallel orientation to the metal surface with a view to increasing the contact. From published studies, for adsorption energies with negative sign, higher values correspond to stronger the interaction of inhibitor molecules with CS surfaces [61,62]. Data available in Table 6, shows that the sequence of adsorption energy is BHMB > HMPB which is consistent with laboratory results obtained for the two compounds.

4. Conclusion

Two selected benzimidazole-2-ones derivatives of 8-hydroxyquinoline have been synthesized and identified by various spectroscopic methods and their performance against corrosion of CS in 1 M HCl investigated using various experimental and theoretical techniques. Results obtained from Tafel analyses indicates that the chemical structure of selected benzimidazole-2-one derivatives of 8-

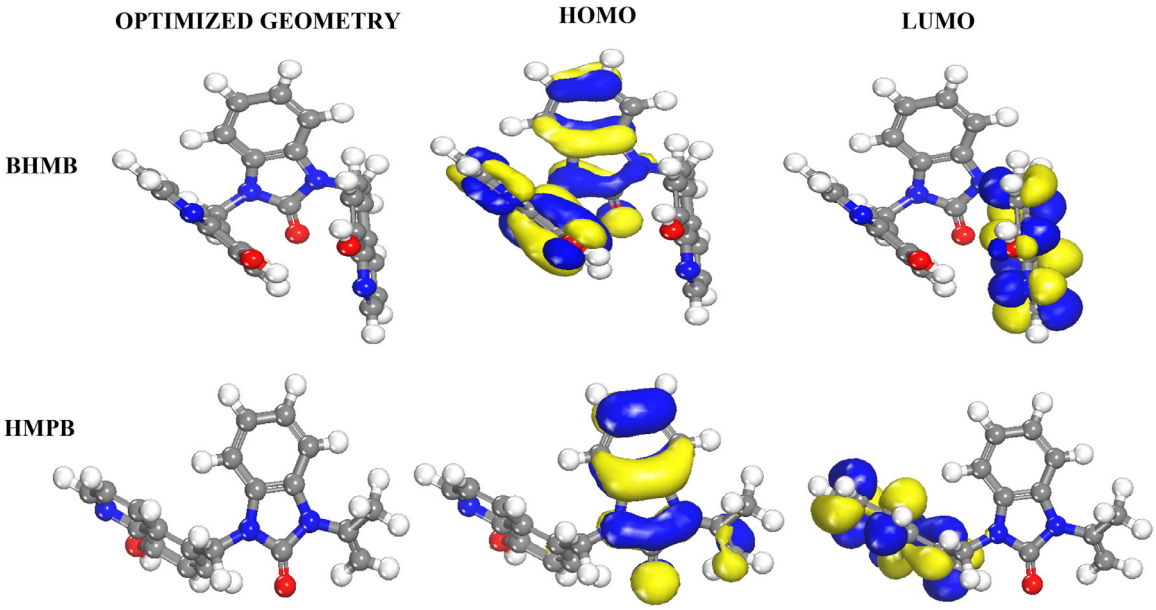

Fig. 20. Optimized geometric structures and molecular orbitals for BHMB and HMPB at the GGA/PBE/DNP level of theory.

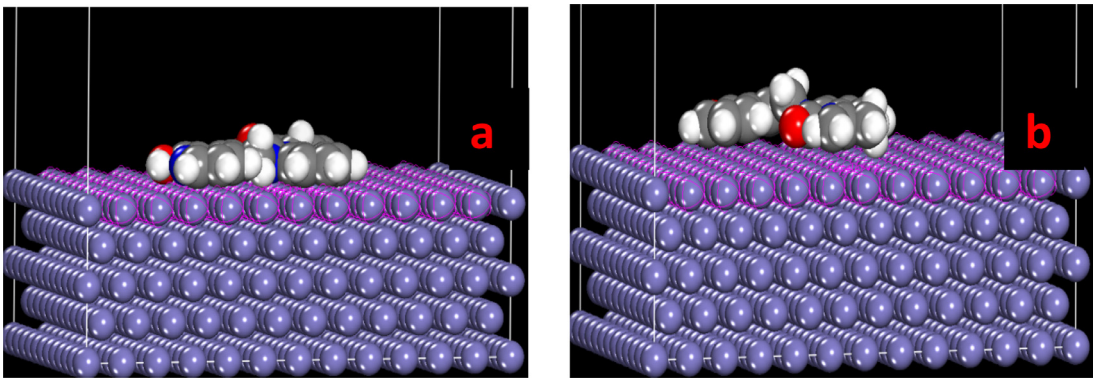

Fig. 21. Stable equilibrium configuration of (a) BHMB and (b) HMPB adsorption on Fe (110) surface utilizing Monte Carlo simulation methodology.

Table 6
The retrieved data on the basis of Monte Carlo simulation for BHMB and HMPB adsorption on Fe (110) surface (kcal/ mole).

Systems	Adsorption Energy	Performance ability, η_{EIS} (%) at 10^{-6} M
Fe (110) + BHMB	−226.38	87.84
Fe (110) + HMPB	−175.16	84.95

hydroxyquinoline has an influence on the inhibiting efficiency. The Tafel result also showed that BHMB and HMPB act as cathodic-type corrosion inhibitors. In general, the gravimetric and electrochemical methods adopted in this study are in reasonable agreement. One semicircle, corresponding to one time constant, was observed in the impedance spectra with the introduction of BHMB, HMPB and the EIS measurements showed an increase of R_p and the decrease of double layer capacitance with increase in concentration of studied inhibitors. The adsorption process of BHMB and HMPB follows the Langmuir adsorption isotherm. The electronic absorption spectra of UV − visible after immersion confirm complex formation of studied compounds with iron ions from CS surface. Results from the experiments and computational data are in reasonable agreement confirming that BHMB is a better corrosion inhibitor than HMPB.

Conflict of interest

No conflict of interest exists, or if such conflict exists, the exact nature must be declared.

Acknowledgements

Ime Bassey Obot acknowledges the Center of Research Excellence in Corrosion (CoRE–C), at the Research Institute, King Fahd University of Petroleum and Minerals, Saudi Arabia for providing the computational softwares for the work described in this manuscript.

Supplementary materials

Supplementary material associated with this article can be found, in the online version, at doi:10.1016/j.surfin.2019.01.005.

References

[1] E.S. Ivanov, Inhibitors for metal corrosion in acid media, Metall. Mosc. 34 (1986) 1990–1997.
[2] H. Zarrok, A. Zarrouk, B. Hammouti, R. Salghi, F. Bentiss, Corrosion control of carbon steel in phosphoric acid by purpald–weight loss, electrochemical and XPS studies, Corros. Sci. 64 (2012) 243–252.
[3] M. E.Mashuga, L.O. Olasunkanmi, E.E. Ebenso, Experimental and theoretical investigation of the inhibitory effect of new pyridazine derivatives for the corrosion of

mild steel in 1M HCl, J. Mol. Struct. 1136 (2017) 127–139.
[4] T.N.J.I. Edison, R. Atchudan, A. Pugazhendhi, Y.R. Lee, M.G. Sethuraman, Corrosion inhibition performance of spermidine on mild steel in acid media, J. Mol. Liq. 264 (2018) 483–489.
[5] S.K. Saha, M. Murmu, N.C. Murmu, P. Banerjee, Evaluating electronic structure of quinazolinone and pyrimidinone molecules for its corrosion inhibition effectiveness on target specific mild steel in the acidic medium: a combined DFT and MD simulation study, J. *Mol. Liq.* 224 (2016) 629–638.
[6] L.O. Olasunkanmi, I.B. Obot, E.E. Ebenso, Adsorption and corrosion inhibition properties of *N*-{n-[1-R-5-(quinoxalin-6-yl)-4,5-dihydropyrazol-3-yl] phenyl} methanesulfon-amides on mild steel in 1M HCl: experimental and theoretical studies, RSC Adv. 6 (90) (2016) 86782–86797.
[7] M. Yadav, R.R. Sinha, T.K. Sarkar, N. Tiwari, Corrosion inhibition effect of pyrazole derivatives on mild steel in hydrochloric acid solution, J. Adhes. Sci. Technol. 29 (16) (2015) 1690–1713.
[8] S. Benabid, T. Douadi, S. Issaadi, C. Penverne, S. Chafaa, Electrochemical and DFT studies of a new synthesized Schiff base as corrosion inhibitor in 1M HCl, Measurement 99 (2017) 53–63.
[9] H.L. Wang, R.B. Liu, J. Xin, Inhibiting effects of some mercapto-triazole derivatives on the corrosion of mild steel in 1.0M HCl medium, Corros. Sci. 46 (10) (2004) 2455–2466.
[10] A.S. Fouda, A.A. Al-Sarawy, E.E. El-Katori, Pyrazolone derivatives as corrosion inhibitors for C-steel in hydrochloric acid solution, Desalination 201 (1-3) (2006) 1–13.
[11] A. Popova, M. Christov, S. Raicheva, E. Sokolova, Adsorption and inhibitive properties of benzimidazole derivatives in acid mild steel corrosion, Corros. Sci. 46 (6) (2004) 1333–1350.
[12] M. Bouklah, N. Benchat, B. Hammouti, A. Aouniti, S. Kertit, Thermodynamic characterisation of steel corrosion and inhibitor adsorption of pyridazine compounds in 0.5M H_2SO_4, Mater. Lett. 60 (15) (2006) 1901–1905.
[13] A. Chaussé, M.M. Chehimi, J.P. Karsi, F. Podvorica, C. Vautrin-Ul.The electrochemical reduction of diazonium salts on iron electrodes, the formation of covalently bonded organic layers and their effect on corrosion, Chem. Mater. 14 (1) (2002) 392–400.
[14] A.A. Spasov, I.N. Yozhitsa, L.I. Bugaeva, V.A. Anisimova, Benzimidazole derivatives: Spectrum of pharmacological activity and toxicological properties (a review), Pharm. Chem. J. 33 (5) (1999) 232–243.
[15] C. Boullais, C. Crouzel, A. Syrota, Synthesis of 4-(3-t-butylamino-2-hydroxypropoxy) -benzimidazol-2(11c)-one, J. Label. Compd. Radiopharm. 23 (5) (1986) 565–567.
[16] M. Ogawa, K. Hatano, Y. Kawasumi, K. Ishiwata, K. Kawamura, S. Ozaki, K. Ito, Synthesis and evaluation of 1-[(3*R*,4*R*)-1-*cyclooctylmethyl*-3-*hydroxymethyl*-4-*piperidyl*]-3-[11C] ethyl-1,3-dihydro-2H-benzimidazol-2-one as a brain ORL1 receptor imaging agent for positron emission tomography, Nucl. Med. Biol. 30 (1) (2003) 51–59.
[17] K. Lutfy, A. Cowan, Buprenorphine: a unique drug with complex pharmacology, Curr. Neuropharmacol. 2 (4) (2004) 395–402.
[18] R. Touir, A. Belakhmima, M.E. Touhami, L. Lakhrissi, M. El Fayed, B. Lakhrissi, E.M. Essassi, Comparative inhibition study of mild steel corrosion in hydrochloric acid by benzimidazole derivatives, J. Mater. Environ. Sci. 4 (6) (2013) 921–930.
[19] L. Lakhrissi, B. Lakhrissi, R. Touir, M.E. Touhami, M. Massoui, E.M. Essassi, Mild steel corrosion inhibition in 200ppm NaCl by new surfactant derivatives of bis-gluco benzimidazolones, Arab. J. Chem. 10 (2017) S3142–S3149.
[20] M. Khan, T.G. Kazi, H.I. Afridi, M. Bilal, A. Akhtar, N. Ullah, S. Talpur, Application of ultrasonically modified cloud point extraction method for simultaneous enrichment of cadmium and lead in sera of different types of gallstone patients, Ultrason. Sonochem. 39 (2017) 313–320.
[21] Z. Dahaghin, H.Z. Mousavi, S.M. Sajjadi, Synthesis and Application of Magnetic Graphene Oxide Modified with 8-Hydroxyquinoline for Extraction and Preconcentration of Trace Heavy Metal Ions, Chem. Select. 2 (3) (2017) 1282–1289.
[22] G. Achary, H.P. Sachin, Y.A. Naik, T.V. Venkatesha, The corrosion inhibition of mild steel by 3-formyl-8-hydroxy quinoline in hydrochloric acid medium, Mater. Chem. Phys. 107 (1) (2008) 44–50.
[23] Y. Abboud, A. Abourriche, T. Saffaj, M. Berrada, M. Charrouf, A. Bennamara, H. Hannache, A novel azo dye, 8-quinolinol-5-azoantipyrine as corrosion inhibitor for mild steel in acidic media, Desalination 237 (2009) 175–189.
[24] M. El Faydy, M. Galai, A. El Assyry, A. Tazouti, R. Touir, B. Lakhrissi, M. Ebn Touhami, A. Zarrouk, Experimental investigation on the corrosion inhibition of carbon steel by 5-(chloromethyl)-8-quinolinol hydrochloride in hydrochloric acid solution, J. Mol. Liq. 219 (2016) 396–404.
[25] L. Feng, X. Wang, Z. Chen, Study on the noncovalent complexes of ginsenoside and cytochrome by electrospray ionization mass spectrometry, Spectrochim. Acta Part A. 71 (2008) 312–316.
[26] D. Mondieig, Ph. Negrier, J.M. Leger, L. Lakhrissi, A. El Assyry, B. Lakhrissi, E.M. Essassi, B. Benali, A. Boucetta, Synthesis and structural study of N-isopropenylbenz-imidazolone, Russ. J. Phys. Chem. A. 89 (5) (2015) 807–811 b) M. A.
[27] B. Lakhrissi, A. Benksim, M. Massoui, E.M. Essassi, V. Lequart, N. Joly, D. Beaupère, A. Wadouachi, P. Martin, Towards the synthesis of new benzimidazolone derivatives with surfactant properties, Carbohydr. Res. 343 (2008) 421–433 L.B. Townsend, R.V. Devivar, S.R. Turk, R. M. Nassiri, J.C. Drach, Synthesis, and antiviral activity of certain 2,5,6-trihalo-1-(beta-D-ribofuranosyl)benzimidazoles, J. Med. Chem. 38 (1995) 4098–4105.
[28] Standard, ASTM, G1-03. Standard practice for preparing, cleaning, and evaluating corrosion test specimens, Annual Book of ASTM Standards 3 (2003), pp. 17–25.
[29] M.T. Alhaffar, S.A. Umoren, I.B. Obot, S.A. Ali, Isoxazolidine derivatives as corrosion inhibitors for low carbon steel in HCl solution: experimental, theoretical and effect of KI studies, RSC Adv. 8 (2018) 1764–1777.
[30] M. Bouanis, M. Tourabi, A. Nyassi, A. Zarrouk, C. Jama, F. Bentiss, Corrosion inhibition performance of 2, 5-bis (4-dimethylaminophenyl)-1, 3, 4-oxadiazole for carbon steel in HCl solution: gravimetric, electrochemical and XPS studies, Appl. Surf. Sci. 389 (2016) 952–966.
[31] M. Tourabi, A. Sahibed-dine, A. Zarrouk, I.B. Obot, B. Hammouti, A.N. F.Bentiss, 3,5-Diaryl-4-amino-1,2,4-triazole derivatives as effective corrosion inhibitors for mild steel in hydrochloric acid solution: correlation between anti-corrosion activity and chemical structure, Prot. Met. Phys. Chem. 53 (3) (2017) 548–559.
[32] A. Singh, K.R. Ansari, M.A. Quraishi, Y. Lin, Synthesis and investigation of pyran derivatives as acidizing corrosion inhibitors for N80 steel in hydrochloric acid: theoretical and experimental approaches, J. Alloy. Compd. 762 (2018) 347–362.
[33] B. Xu, W. Yang, Y. Liu, X. Yin, W. Gong, Y. Chen, Experimental and theoretical evaluation of two pyridine carboxaldehyde thiosemicarbazone compounds as corrosion inhibitors for mild steel in hydrochloric acid solution, Corros. Sci. 78 (2014) 260–268.
[34] S.K. Saha, M. Murmu, N. C., I. Murmu, B. Obot, P. Banerjee, Molecular level insights for the corrosion inhibition effectiveness of three amine derivatives on the carbon steel surface in the adverse medium: a combined density functional theory and molecular dynamics simulation study, Surf. Interfaces 10 (2018) 65–73.
[35] R. Solmaz, G. Kardaş, B. Yazıcı, M. Erbil, Adsorption and corrosion inhibitive properties of 2-amino-5-mercapto-1,3,4-thiadiazole on mild steel in hydrochloric acid media, Coll. Surf. A Physicochem. Eng. Asp. 312 (1) (2008) 7–17.
[36] M. El Achouri, S. Kertit, H.M. Gouttaya, B. Nciri, Y. Bensouda, L. Perez, M.R. Infante, K. Elkacemi, Corrosion inhibition of iron in 1M HCl by some gemini surfactants in the series of alkanediyl-α,ω-bis-(dimethyl tetradecyl ammonium bromide), Prog. Org. Coat. 43 (2001) 267–273.
[37] M. Hosseini, S.F.L. Mertens, M. Ghorbani, M.R. Arshadi, Asymmetrical Schiff bases as inhibitors of mild steel corrosion in sulphuric acid media, Mater. Chem. Phys. 78 (2003) 800–808.
[38] D.K. Yadav, D.S. Chauhan, I. Ahamad, M.A. Quraishi, Electrochemical behavior of steel/acid interface: Adsorption and inhibition effect of oligomeric aniline, RSC Adv. 3 (2) (2013) 632–646.
[39] M. Kissi, M. Bouklah, B. Hammouti, M. Benkaddour, Establishment of equivalent circuits from electrochemical impedance spectroscopy study of corrosion inhibition of steel by pyrazine in sulphuric acidic solution, Appl. Surf. Sci. 252 (2006) 4190–4197.
[40] A.M. Fekry, The influence of chloride and sulphate ions on the corrosion behavior of Ti and Ti-6Al-4V alloy in oxalic acid, Electrochim. Acta 54 (2009) 3480–3489.
[41] H. Zarrok, H. Oudda, A. El Midaoui, A. Zarrouk, B. Hammouti, M. Ebn Touhami, A. Attayibat, S. Radi, R. Touzani, Some new bipyrazole derivatives as corrosion inhibitors for C38 steel in acidic medium, Res. Chem. Intermed. 38 (2012) 2051–2063.
[42] A. Popova, M. Christov, Evaluation of impedance measurements on mild steel corrosion in acid media in the presence of heterocyclic compounds, Corros. Sci. 48 (10) (2006) 3208–3221.
[43] A. Zarrouk, B. Hammouti, T. Lakhlifi, M. Traisnel, H. Vezin, F. Bentiss, New 1H-pyrrole-2,5-dione derivatives as efficient organic inhibitors of carbon steel corrosion in hydrochloric acid medium: electrochemical, XPS and DFT studies, Corros. Sci. 90 (2015) 572–584.
[44] M. Elfaydy, H. Lgaz, R. Salghi, M. Larouj, S. Jodeh, M. Rbaa, H. Oudda, K. Toumiat, B. Lakhrissi, Investigation of corrosion inhibition mechanism of quinoline derivative on mild steel in 1.0M HCl solution: experimental, theoretical and Monte Carlo simulation, J. Mater. Environ. Sci. 7 (2016) 3193–3210.
[45] M. El Faydy, M. Galai, R. Touir, A. El Assyry, M. Ebn Touhami, B. Benali, B. Lakhrissi, A. Zarrouk, Experimental and theoretical studies for steel XC38 corrosion inhibition in 1M HCl by N-(8-hydroxyquinolin-5-yl)-methyl)-N-phenylacetamide, J. Mater. Environ. Sci. 7 (2016) 1406–1416.
[46] M.S. Morad, Inhibition of iron corrosion in acid solutions by Cefatrexyl: Behaviour near and at the corrosion potential, Corros. Sci. 50 (2008) 436–448.
[47] L. Boucherit, T. Douadi, N. Chafai, M. Al-Noaimi, S. Chafaa, The inhibition Activity of 1, 10-bis (2-formylphenyl)-1, 4, 7, 10-tetraoxadecane (Ald) and its Schiff base (L) on the corrosion of carbon steel in HCl: experimental and theoretical studies, Int. J. Electrochem. Sci. 13 (2018) 3997–4025.
[48] Q. Ma, 1, 2, 3-triazole derivatives as corrosion inhibitors for mild steel in acidic medium: experimental and computational chemistry studies, Corros. Sci. 129 (2017) 91–101.
[49] A. Popova, M. Christov, A. asilev, Mono-and dicationic benzothiazolic quaternary ammonium bromides as mild steel corrosion inhibitors. Part III: influence of the temperature on the inhibition process, Corros. Sci. 94 (2015) 70–78.
[50] H. Tayebi, H. Bourazmi, B. Himmi, A. El Assyry, Y. Ramli, A. Zarrouk, B. Hammouti, Combined electrochemical and quantum chemical study of new quinoxaline derivative as corrosion inhibitor for carbon steel in acidic media, Der Pharm. Chem. 6 (2014) 220–234.
[51] J. O'M. Bockris, A.K.N. Reddy, Modern Electrochemistry 2 Plenum Press, New York, 1977.
[52] H. Zarrok, H. Oudda, A. El Midaoui, A. Zarrouk, B. Hammouti, M.E. Touhami, R. Touzani, Some new bipyrazole derivatives as corrosion inhibitors for C38 steel in acidic medium, Res. Chem. Intermed. 38 (8) (2012) 2051–2063.
[53] F. Zhang, Y. Tang, Z. Cao, W. Jing, Z. Wu, Y. Chen, Performance and theoretical study on corrosion inhibition of 2-(4-pyridyl)-benzimidazole for mild steel in hydrochloric acid, Corros. Sci. 61 (2012) 1–9.
[54] G.E. Badr, The role of some thio semicarbazide derivatives as corrosion inhibitors for C-steel in acidic media, Corros. Sci. 51 (2009) 2529–2536.
[55] P. Mourya, P. Singh, A.K. Tewari, R.B. Rastogi, M.M. Singh, Relationship between structure and inhibition behaviour of quinolinium salts for mild steel corrosion:

Experimental and theoretical approach, Corros. Sci. 95 (2015) 71–87.
[56] A. Yurt, A. Balaban, S.U. Kandemir, G. Bereket, B. Erk, Investigation on some Schiff bases as HCl corrosion inhibitors for carbon steel, Mater. Chem. Phys. 85 (2004) 420–426.
[57] B.G. Ateya, B.E. El-Anadouli, F.M. El-Nizamy, The adsorption of thiourea on mild steel, Corros. Sci. 24 (6) (1984) 509–515.
[58] K. Minami, T. Ohashi, M. Suzuki, T. Aizawa, T. Adschiri, K. Arai, Estimation of local density augmentation and hydrogen bonding between pyridazine and water under sub-and supercritical conditions utilizing UV-vis spectroscopy, Anal. Sci. 22 (2006) 1417–1423.
[59] I.B. Obot, E.E. Ebenso, M.M. Kabanda, Metronidazole as environmentally safe corrosion inhibitor for mild steel in 0.5M HCl: Experimental and theoretical investigation, J. Environ. Chem. Eng. 1 (2013) 431–439.
[60] I.B. Obot, S.A. Umoren, Z.M. Gasem, R. Suleiman, B. El Ali, Theoretical prediction and electrochemical evaluation of vinylimidazole and allylimidazole as possible green corrosion inhibitors for carbon steel in 1M HCl, J. Ind. Eng. Chem. 21 (2015) 1328–1339.
[61] J.P. Zeng, J.Y. Zhang, X.D. Gong, Molecular dynamics simulation of interaction between benzotriazoles and cuprous oxide crystal, Comput. Theor. Chem. 963 (1) (2011) 110–114.
[62] L. Guo, S. Zhu, S. Zhang, Q. He, W. Li, Theoretical studies of three triazole derivatives as corrosion inhibitors for mild steel in acidic medium, Corros. Sci. 87 (2014) 366–375.